PROPAGATION CHARACTERISTICS OF OPTICAL FIBRES - RADIATION LOSS AND MODE CONVERSION FROM A LOCALIZED INHOMOGENEITY IN A CLADDED FIBRE

Covering Period 1st May, 1973 to 30th April, 1974.

G.L. Yip, J. Martucci and J.C.Y. Huang
Department of Electrical Engineering,
McGill University,
Montreal, Quebec.

McGILL UNIVERSITY

MONTREAL

Report No. 3 to

Department of Supply and Serives Ottawa

on Contract SP2.36100-3-0-0340

Serial 0SP3-0132

(2)

PROPAGATION CHARACTERISTICS OF OPTICAL FIBRES - RADIATION LOSS AND MODE CONVERSION FROM A LOCALIZED INHOMOGENEITY IN A CLADDED FIBRE

Covering Period 1st May, 1973 to 30th April, 1974.

G.L. Yip, J. Martucci and J.C.Y. Huang
Department of Electrical Engineering,
McGill University,
Montreal, Quebec.

Prepared for
Communications Research Centre,
Shirley Bay, Ottawa, Ontario.

May, 1974.

TABLE OF CONTENTS

ABSTRACT

This report considers the radiation and mode conversion losses in the cladded fiber due to a scattering center located on or near the fiber axis.

The other loss mechanism, namely absorption loss by metallic impurities (e.g. Fe, Cu), had been treated in detail (see Report No. 2 to the Department of Supply and Services, Ottawa on Contract No. 01GR 36100-2-0204, Serial No. OGR2-0163).

The radiation loss due to a scattering center was also treated in the same report. A summary of the materials is included here to provide some continuity of this report because radiation loss and mode conversion loss are closely related.

A discussion to determine the minimum bend radius by the critical angle criterion is also presented.

1. Introduction

Our attention is focused on impurities in the fiber or fiber inhomogeneities as scattering centers on or near the fiber axis.

For most operational purposes, the dominant HE_{11} mode is used in a single-mode cladded fiber. When it impinges upon a scattering center, whose overall dimension is very much smaller than the wavelength, a current moment will be induced, and this will scatter power into radiation and surface waves (both "leaky" and "propagating" modes).

Fig. 1 depicts the situation under our consideration. As we can see, some of the scattered power is radiated out of the cladded fiber. Some of the scattered power is converted into higher-order modes and guided along the fiber. If these higher-order modes encounter another scattering center, some of the power will be reconverted into lower-order modes and back into the original HE_{11} mode. This phenomenon is called mode conversion and reconversion. Radiation just causes a loss of power; while mode conversion and reconversion will cause signal distortion. This is because higher-order modes are travelling with different velocities. When reconversion happens, this will cause intercoupling between these modes.

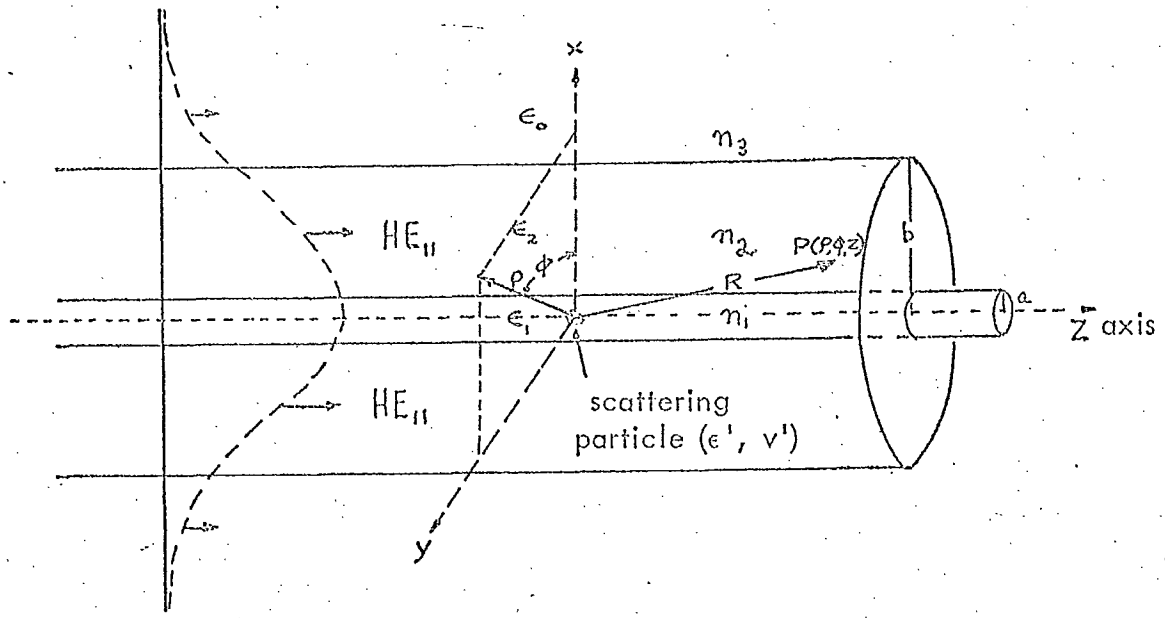

(a) HE_{11} modal power incident on scattering particle (ϵ', ν').

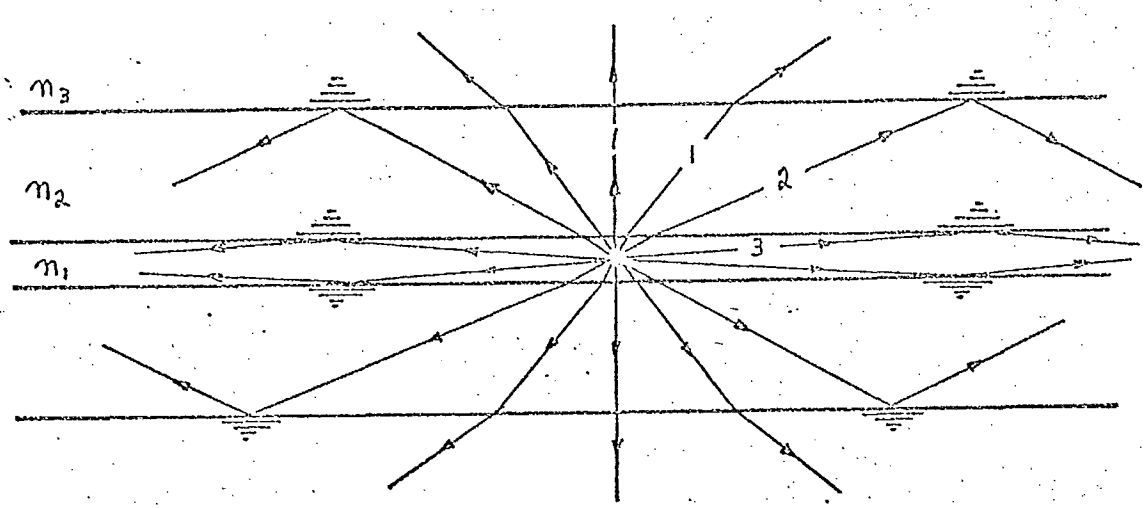

(b) Modes excited by scattering particle :

[1] ——— radiating mode

[2,3] ——— guided cladding and core modes

FIGURE 1 Scattering from a Small Particle (ϵ', ν') on the Fibre Axis.

Marcuse[1,2] studied mode conversion caused by surface imperfection of a dielectric slab waveguide and also mode conversion caused by diameter change of a round dielectric waveguide. Perturbation of the geometry of waveguide was assumed to compute the total exchange of energy from the lowest order to the next higher order mode.

Clarricoats and Chan[3] have analyzed the situation of a scattering center located inside the cladded fiber by assuming infinite cladding and, by assuming a small dielectric difference between the scatterer and the core region (or the cladding region) computed the mode conversion power in terms of the incident HE_{11} mode. Radiation power was also computed.

The method of analysis used in this report is based on the paper by Yip[4] in studying the launching efficiency of the HE_{11} mode on a dielectric rod. This method was further employed for the study of the launching efficiency of the HE_{11} mode on a dielectric tube by Yip and Au-yang[5]. The technique involves expressing the sources and fields in a Fourier integral in the z-direction and a Fourier series in the φ- direction. Though, in general, the Green's function for an open-bounded cylindrical structure is extremely complex, for the simpler case of a transversely-oriented infinitesimal dipole on the axis of a cladded fiber, the Green's function is available.

A current moment will be induced on the scatterer when the incident dominant HE_{11} mode impinges upon it. This will make the scatterer appear as

an electric dipole (Rayleigh scattering). Suitable fields must then satisfy the Maxwell's equations with boundary conditions met at the interface between the core and the cladding, and between the cladding and the outer air regions.

Radiation and surface waves would be excited and can be computed. The magnitude of the induced current moment depends on the field of the incident mode.

2. Method of Analysis

The cladded fibre as pictured in Fig. 1 is assumed lossless, characterized by a permittivity of $\epsilon_1 = \epsilon_o \bar{\epsilon}_1$ in the core with radius a, *and* by a permittivity of $\epsilon_2 = \epsilon_o \bar{\epsilon}_2$ in the cladding with radius b. Both have a permeability μ_o. The surrounding free space is characterized by the permittivity ϵ_o and the permeability μ_o.

As explained in the introduction, the point dipole is placed at the origin of the coordinate system, and oriented perpendicular to the z-axis. The time dependence is assumed to be e^{-iwt}, and the induced current density on the point dipole is specified by a normalized delta function:

$$J = \hat{x}\, J_e \left[\frac{\delta(\rho)\,\delta(z)}{2\pi\rho} \right] \tag{2.1}$$

where J_e = the induced current moment of the point dipole.

In the core region $0 < \rho < a$, the normalized electric and magnetic fields must satisfy the following Maxwell's equations:

$$\begin{aligned} \nabla \times \underline{E} &= i K_o \underline{H} \\ \nabla \times \underline{H} &= -i K_o \epsilon_1 \underline{E} + \underline{J} \end{aligned} \tag{2.2}$$

where $\underline{E} = \sqrt{\epsilon_o}\, \underline{E}_1$, $\underline{H} = \sqrt{\mu_o}\, \underline{H}_1$, and $\underline{J} = \sqrt{\mu_o}\, \underline{J}_1$

with subscripted quantities representing the normalized fields and currents.

$k_o = \dfrac{2\pi}{\lambda_o}$ free-space propagation constant.

By the Fourier transform technique, the actual fields can be represented as

$$f(\rho,\phi,z) = \frac{k_o}{2\pi}\int_{-\infty}^{\infty} F(\rho,\phi,\gamma)\, e^{ik_o\gamma z}\, d\gamma \tag{2.3}$$

where $\gamma = \bar{\beta} = \frac{\beta}{k_o}$ normalized propagation constant.

The transformed fields $F(\rho, \varphi, \gamma)$ are further expressed in a Fourier series:

$$F(\rho,\phi,\gamma) = \sum_{m=-\infty}^{\infty} F_m(\rho,\gamma)\, e^{im\phi} \tag{2.4}$$

In the source-free region inside the fibre core $0 < \rho < a$:

$$\begin{bmatrix} E_{\rho 1}(\rho,\phi,\gamma) \\ E_{\phi 1}(\rho,\phi,\gamma) \end{bmatrix} = -\frac{i}{k_o\eta_1^2}\begin{bmatrix} i\gamma\frac{\partial}{\partial\rho} & -\frac{1}{\rho}\frac{\partial}{\partial\phi} \\ i\gamma\frac{\partial}{\partial\phi} & \frac{\partial}{\partial\rho} \end{bmatrix}\begin{bmatrix} iE_{z1}(\rho,\phi,\gamma) \\ H_{z1}(\rho,\phi,\gamma) \end{bmatrix}$$

$$\begin{bmatrix} H_{\rho 1}(\rho,\phi,\gamma) \\ H_{\phi 1}(\rho,\phi,\gamma) \end{bmatrix} = \frac{1}{k_o\eta_1^2}\begin{bmatrix} -\frac{\bar{\epsilon}_1}{\rho}\frac{\partial}{\partial\phi} & i\gamma\frac{\partial}{\partial\rho} \\ \bar{\epsilon}_1\frac{\partial}{\partial\rho} & i\frac{\gamma}{\rho}\frac{\partial}{\partial\phi} \end{bmatrix}\begin{bmatrix} iE_{z1}(\rho,\phi,\gamma) \\ H_{z1}(\rho,\phi,\gamma) \end{bmatrix} \tag{2.5}$$

where $\eta_1 = \sqrt{\bar{\epsilon}_1 - \gamma^2}$

With these and Maxwell's equations, the longitudinal field components in the core satisfy the following wave equations:

$$\nabla_t^2 \begin{bmatrix} H_{z1}(\rho,\gamma) \\ iE_{z1}(\rho,\gamma) \end{bmatrix} + k_o^2\eta_1^2 \begin{bmatrix} H_{z1}(\rho,\gamma) \\ iE_{z1}(\rho,\gamma) \end{bmatrix} \tag{2.6a}$$

$$= \frac{1}{2} J_e\sqrt{\mu_o}\,\frac{\partial}{\partial\rho}\left(\frac{\delta(\rho)}{2\pi\rho}\right)\left\{\begin{bmatrix} -1 \\ \gamma\sqrt{\bar{\epsilon}_1} \end{bmatrix} e^{i\phi} + \begin{bmatrix} 1 \\ \gamma\sqrt{\bar{\epsilon}_1} \end{bmatrix} e^{-i\phi}\right\}$$

From (2.6), we can clearly see that only $m = \pm 1$ modes will be excited.

The wave equations are also true for the cladding and the free-space regions with $J_e = o$ and η_1 replaced by $\eta_2 = \sqrt{\epsilon_2 - \gamma^2}$, $\eta_o = \sqrt{1 - \gamma^2}$ respectively.

For $a < \rho < b$

$$\nabla_t^2 \begin{bmatrix} H_{z2}(\rho, \gamma) \\ iE_{z2}(\rho, \gamma) \end{bmatrix} + K_o^2 \eta_2^2 \begin{bmatrix} H_{z2}(\rho, \gamma) \\ iE_{z2}(\rho, \gamma) \end{bmatrix} = 0 \tag{2.6b}$$

For $\rho > b$

$$\nabla_t^2 \begin{bmatrix} H_{z3}(\rho, \gamma) \\ iE_{z3}(\rho, \gamma) \end{bmatrix} + K_o^2 \eta_o^2 \begin{bmatrix} H_{z3}(\rho, \gamma) \\ iE_{z3}(\rho, \gamma) \end{bmatrix} = 0 \tag{2.6c}$$

Our solutions for longitudinal fields in the core $o < \rho < a$ are given by

$$H_{z1,m}(\rho,\gamma) = I\eta_1 [S_m i Y_1(K_0\eta_1\rho) + B_m J_1(K_0\eta_1\rho)]$$

$$i E_{z1,m}(\rho,\gamma) = I\eta_1 [T_m i Y_1(K_0\eta_1\rho) + A_m J_1(K_0\eta_1\rho)] \tag{2.7}$$

where $S_m = -\frac{mi}{2}$ and $T_m = \frac{i\gamma}{2\bar{\epsilon}_1}$

As mentioned in the earlier contract report (Report No. 1 to the Department of Supply and Services, Ottawa on contract No. 01GR 36001-1-0519, Serial No. 0GRI-104), there are two regions of interest to be accounted for in the dispersion characteristics (see Fig. 2).

In the domain where the normalized propagation constant $1 < \gamma < \sqrt{\epsilon}_2$, both $\eta_1 = \sqrt{\epsilon}_1 - \gamma^2$ and $\eta_2 = \sqrt{\epsilon}_2 - \gamma^2$ are real. In this case (Case 1), we have the so-called "leaky" modes, or "cladding" modes as the waves are mostly propagating in the cladding.

In the domain where the normalized propagation constant $\sqrt{\epsilon}_2 < \gamma < \sqrt{\epsilon}_1$, $\eta_1 = \sqrt{\epsilon}_1 - \gamma^2$ is still real, while $\eta_2 = \sqrt{\epsilon}_2 - \gamma^2$ becomes imaginary. This (Case 2) gives rise to the so-called "propagating" modes, or "core" modes, as most of the waves are propagating in the core.

In the cladding $a < \gamma < b$, the longitudinal fields should be given according to the two cases mentioned in the last paragraph.

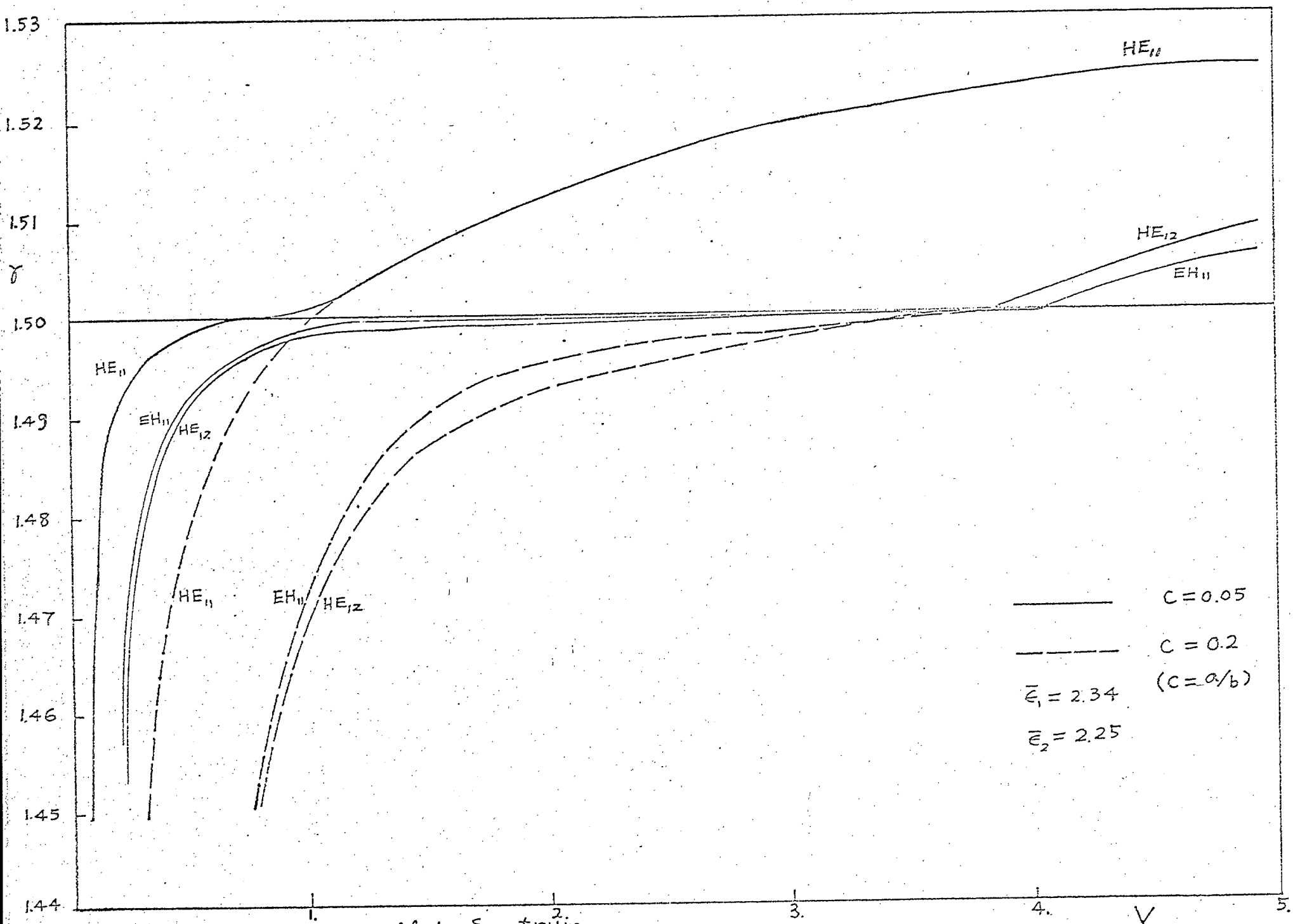

Fig 2. Mode Spectrum

Case 1: For η_1 and η_2 both real ("leaky" modes),

$$H_{z2,m}(\rho,\gamma) = I\eta_2\left[C_m Y_1(K_0\eta_2\rho) + D_m J_1(K_0\eta_2\rho)\right]$$

$$iE_{z2,m}(\rho,\gamma) = I\eta_2\left[E_m Y_1(K_0\eta_2\rho) + F_m J_1(K_0\eta_2\rho)\right] \tag{2.8a}$$

Case 2: For η_1 real and η_2 imaginary ("propagating" modes),

$$H_{z2,m}(\rho,\gamma) = I|\eta_2|\left[C'_m K_1(K_0|\eta_2|\rho) + D'_m I_1(K_0|\eta_2|\rho)\right]$$

$$iE_{z2,m}(\rho,\gamma) = I|\eta_2|\left[E'_m K_1(K_0|\eta_2|\rho) + F'_m I_1(K_0|\eta_2|\rho)\right] \tag{2.8b}$$

In the free space $\rho > b$ where $\eta_o = \sqrt{1-\gamma^2}$, the longitudinal fields are given by:

$$H_{z3,m}(\rho,\gamma) = I\eta_o G_m H_1^{(1)}(K_0\eta_0\rho)$$

$$iE_{z3,m}(\rho,\gamma) = I\eta_o L_m H_1^{(1)}(K_0\eta_0\rho) \tag{2.9}$$

The eight coefficients A_m's are excitation coefficients and can be determined by matching the tangential field components at $\rho = a, b$. This is given in matrix forms:

$$[M]\,[V] = [S] \tag{2.10}$$

The details of the matrix components for the case where both η_1 and η_2 are real are given in table I. $X = k_o\,\eta_1\,a$, $V = k_o\,\eta_2\,b$,

$$
\underset{M\,(8\times 8)}{\begin{bmatrix}
\eta_1 J_1(X) & -\eta_2 Y_1(cV) & -\eta_2 J_1(cV) & 0 & 0 & 0 & 0 & 0 \\
0 & 0 & 0 & 0 & \eta_1 J_1(X) & -\eta_2 Y_1(cV) & -\eta_2 J_1(cV) & 0 \\
\frac{\gamma m}{\eta_1 a} J_1(X) & \frac{-\gamma m}{\eta_2 a} Y_1(cV) & \frac{-\gamma m}{\eta_2 a} J_1(cV) & 0 & -k_o J_1'(X) & k_o Y_1'(cV) & k_o J_1'(cV) & 0 \\
\bar{\epsilon}_1 k_o J_1'(X) & -\bar{\epsilon}_2 k_o Y_1'(cV) & -\bar{\epsilon}_2 k_o J_1'(cV) & 0 & \frac{-\gamma m}{\eta_1 a} J_1(X) & \frac{\gamma m}{\eta_2 a} Y_1(cV) & \frac{\gamma m}{\eta_2 a} J_1(cV) & 0 \\
0 & \eta_2 Y_1(V) & \eta_2 J_1(V) & -\eta_3 H_1(N) & 0 & 0 & 0 & 0 \\
0 & 0 & 0 & 0 & 0 & \eta_2 Y_1(V) & \eta_2 J_1(V) & -\eta_3 H_1(N) \\
0 & \frac{-\gamma m}{\eta_2 b} Y_1(V) & \frac{-\gamma m}{\eta_2 b} J_1(V) & \frac{\gamma m}{\eta_3 b} H_1(N) & 0 & k_o Y_1'(V) & k_o J_1'(V) & -k_o H_1'(N) \\
0 & -\bar{\epsilon}_2 k_o Y_1'(V) & -\bar{\epsilon}_2 k_o J_1'(V) & k_o' H_1'(N) & 0 & \frac{\gamma m}{\eta_2 b} Y_1(V) & \frac{\gamma m}{\eta_2 b} J_1(V) & \frac{-\gamma m}{\eta_3 b} H_1(N)
\end{bmatrix}}
\underset{\underline{v}}{\begin{bmatrix} A_m \\ E_m \\ F_m \\ L_m \\ B_m \\ C_m \\ D_m \\ G_m \end{bmatrix}}
=
\underset{\underline{S}}{\begin{bmatrix}
-\eta_1 T_m i Y_1(X) \\
-\eta_1 S_m i Y_1(X) \\
\left[S_m k_o i Y_1'(X) \quad \frac{-\gamma m}{\eta_1 a} T_m i Y_1(X) \right] \\
\left[\frac{\gamma m}{\eta_1 a} S_m i Y_1(X) \quad -T_m \bar{\epsilon}_1 k_o i Y_1'(X) \right] \\
0 \\
0 \\
0 \\
0
\end{bmatrix}}
\qquad (2.10)
$$

source column

TABLE I Continuity of Tangential Fields Arranged in Matrix Format $M\,\underline{v} = \underline{S}$.

$N = k_o \eta_o b$, and $W = iN$. For the case where η_1 real and η_2 imaginary, we just change $J_1 \to I_1$, and $Y_1 \to K_1$.

The transverse field components of the transformed fields are derived from the longitudinal fields by Eq. (2.5).

Therefore the actual fields, e.g., $H_{z3}(\rho, \varphi, z)$ and $iE_{z3}(\rho, \varphi, z)$ can be obtained by Fourier transformation:

$$H_{z3}(\rho,\phi,z) = \frac{K_o}{2\pi}\int_{-\infty}^{\infty}\Big[\sum_{m=\pm 1} H_{z3,m}(\rho,\gamma)\, e^{im\phi}\Big] e^{iK_o\gamma z}\, d\gamma$$

$$i\,E_{z3}(\rho,\phi,z) = \frac{K_o}{2\pi}\int_{-\infty}^{\infty}\Big[\sum_{m=\pm 1} iE_{z3,m}(\rho,\gamma)\, e^{im\phi}\Big] e^{iK_o\gamma z}\, d\gamma \qquad (2.11)$$

As explained in the rod case[4], the real poles γ_s can be shown to give rise to surface waves guided and unattenuated along the fibre.

The various coefficients can be conveniently expressed in the following form:

$$Am = \frac{\overline{Am}}{\Delta(\gamma)}, \quad Bm = \frac{\overline{Bm}}{\Delta(\gamma)} \quad \text{etc}$$

where $\Delta(\gamma)$ is the dispersion equation, and is derived from det. [M]. It is interesting to note that det [M] =

$$-\left(\frac{\gamma}{c}\right)^4 c^2 k_o^4 N^2 V^2 \eta_1^2 \eta_2^2 J_1^2(X)\, Y_1^2(V)\, Y_1^2(CV)\, H_1^2(N)\, \Delta(\gamma).$$

Here, $\Delta(\gamma)$ is the dispersion equation of a source-free cladded fiber, and has been derived previously.

3. Radiation Power

For the power radiated, we integrate the real part of the radial component of the complex Poynting vector in Region III over a cylindrical surface of radius ρ greater than b, i.e.,

$$P_r = \frac{1}{2\sqrt{\mu_0 \epsilon_0}} \, Re \int_{-\infty}^{\infty}\int_{0}^{2\pi} \left[E_{\phi 3}(\rho,\phi,z) H_{z3}^{*}(\rho,\phi,z) - E_{z3}(\rho,\phi,z) H_{\phi 3}^{*}(\rho,\phi,z) \right] \rho \, d\phi \, dz$$

$$= \frac{k_0 \rho}{4\pi\sqrt{\mu_0 \epsilon_0}} \, Re \int_{-\infty}^{\infty}\int_{0}^{2\pi} P(\rho,\phi,\gamma) \, d\phi \, d\gamma \qquad \text{using Parseval's Theorem} \tag{3.1}$$

where $P(\rho,\phi,\gamma) = Re\left[E_{\phi 3}(\rho,\phi,\gamma) H_{z3}^{*}(\rho,\phi,\gamma) - E_{z3}(\rho,\phi,\gamma) H_{\phi 3}^{*}(\rho,\phi,\gamma) \right]$

Now for $|\gamma| > 1$, the radial component of the complex Poynting vector is purely imaginary, corresponding to the evanescent guided modes. Hence, these do not contribute to the radiated power. By making the usual far field approximations for the Hankel functions and realizing that $\gamma = \cos\theta$, Eq. (3.1) becomes

$$P_r = J_e^2 \int_0^{2\pi}\int_0^{2\pi} P(\theta,\phi) \, d\phi \, d\theta \tag{3.2}$$

on setting $\gamma = \cos\theta$ and integrating over $|\gamma| \leq 1$

where $$P(\theta,\phi) = \frac{K_o^2}{16\pi^3}\sqrt{\frac{\mu_o}{\epsilon_o}}\left[P_{11} + P_{12}\cos 2\phi - P_{13}\sin 2\phi\right]\sin\phi \qquad (3.3)$$

$$P_{11} = \sum_{m=\pm 1}\left[\,|L_m(\cos\theta)|^2 + |G_m(\cos\theta)|^2\,\right] \qquad (3.4a)$$

$$P_{12} = 2\left[G_{r,1}G_{r,-1} + G_{i,1}G_{i,-1} + L_{r,1}L_{r,-1} + L_{i,1}L_{i,-1}\right] \qquad (3.4b)$$

$$P_{13} = 2\left[G_{i,1}G_{r,-1} - G_{r,1}G_{i,-1} + L_{i,1}L_{r,-1} - L_{r,1}L_{i,-1}\right] \qquad (3.4c)$$

$$L_m(\cos\theta) = L_{r,m} + i\,L_{i,m}$$
$$G_m(\cos\theta) = G_{r,m} + i\,G_{i,m} \qquad m = \pm 1$$

The integrand $P(\theta, \varphi)$ in eq. (3.3) is proportional to the power intensity at angles (θ, φ). Hence $P(\theta,\varphi)$ can be interpreted as the radiation power pattern. It should be noted, however, that the terms P_{12} and P_{13} do not contribute to the radiated power since the azimuthal (φ) integrations are zero for these two terms.

Hence, the total radiated power becomes:

$$P_r = \left(\frac{J_e^2}{2}\right)\frac{K_o^2}{4\pi}\sqrt{\frac{\mu_o}{\epsilon_o}}\sum_{m=\pm 1}\int_0^{\frac{\pi}{2}}\left[\,|L_m(\cos\theta)|^2 + |G_m(\cos\theta)|^2\,\right]d\theta$$

$$= \frac{1}{2}J_e^2 R_r \qquad (3.5)$$

where $$R_r = \frac{K_o^2}{4\pi}\sqrt{\frac{\mu_o}{\epsilon_o}}\sum_{m=\pm 1}\int_0^{\frac{\pi}{2}}\left[\,|L_m(\cos\theta)|^2 + |G_m(\cos\theta)|^2\,\right]d\theta \qquad (3.6)$$

is the radiation resistance of the point source on the fiber axis.

The integral in equation (3.6) is then computed numerically.

In Fig. 3 (a,b,c), we plot the radiation power pattern $P(\theta, \varphi)$ for the three principal planes, i.e., $P(\theta, 0^\circ)$, $P(\theta, 90^\circ)$, and $P(90^\circ, \varphi)$, where each one is normalized with its corresponding maximum value. When $V = 0.1$, there are nulls along the Z- axis (Fig. 3.a, b), as compared to that of a point dipole in free space. This corresponds to the power launched into the guided modes propagating in the Z - axis (both forward and backward). For the case of $V = 1.5$, 2.4 we still have nulls along the Z - axis, but now the power pattern displays many minimums as well. The pattern in the transverse plane of the fiber axis (Fig. 3.c, $P(90^\circ, \varphi)$) is the same as that in free space.

3.1 Fraction of Incident Power Scattered into Radiation by a Small Scattering Volume on the Fiber Axis

The incident HE_{11} power is:

$$P_i(HE_{11}) = \pi b^2 \bar{S}_i(V) A_1^2 \tag{3.7}$$

where πb^2 = cladding area

A_1 = excitation coefficient of HE_{11}

$\bar{S}_i(v)$ = integral expressions of fields

(see eqs. 71 in Report No. 1)

$V = 2\pi \frac{a}{\lambda_o} \sqrt{\bar{\epsilon}_1 - \bar{\epsilon}_2}$, normalized frequency

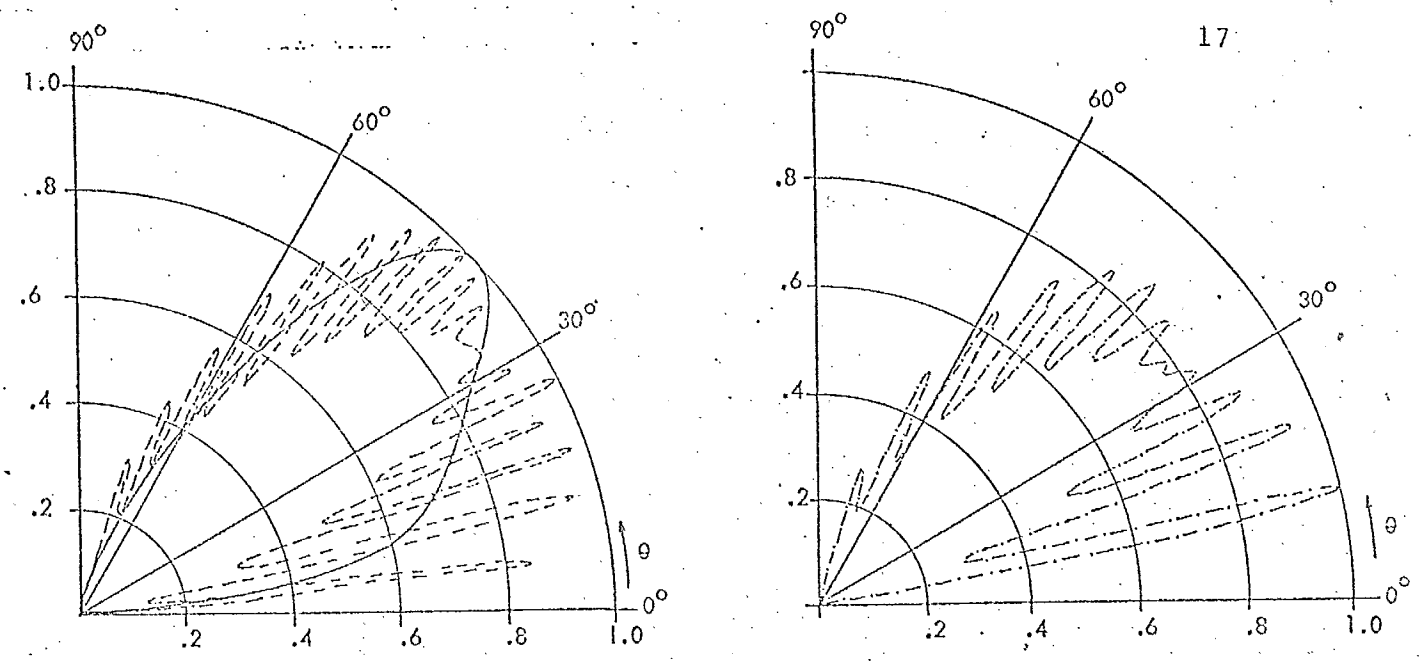

(a) $P(\theta, 0^\circ)$

V = 0.1
V = 1.5
V = 2.4

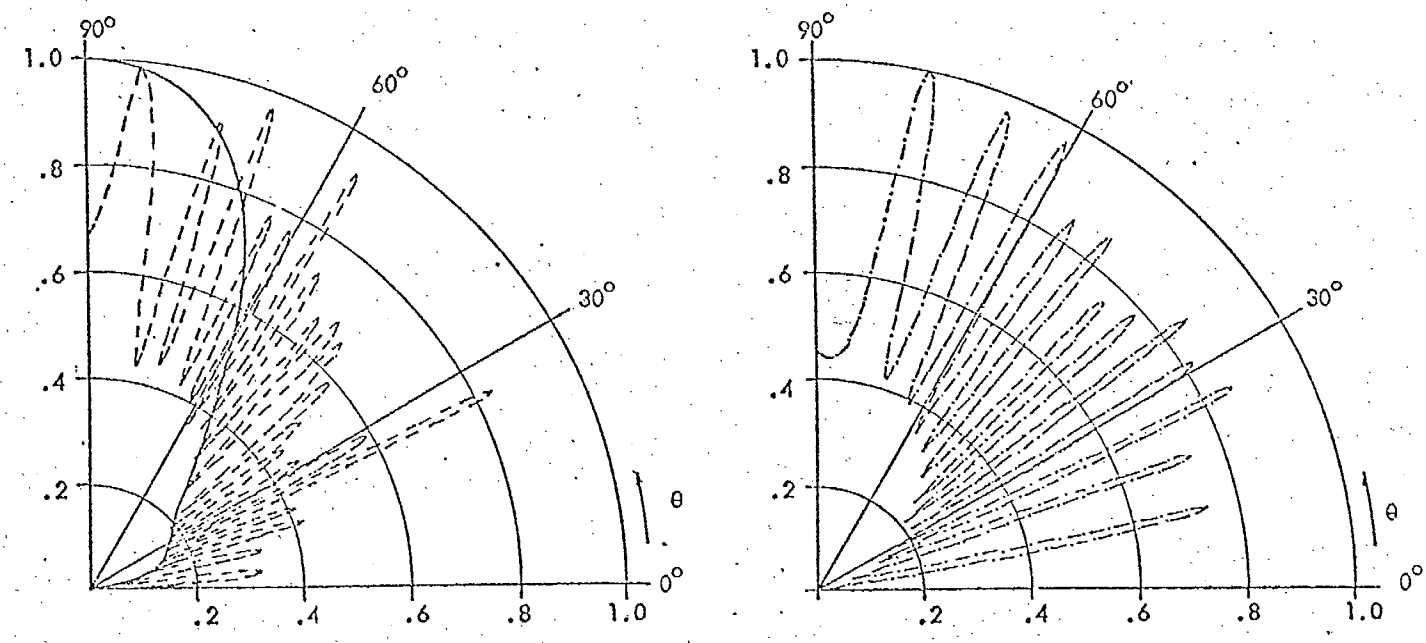

(b) $P(\theta, 90^\circ)$

FIGURE 3.a,b Radiation Power Pattern for $\bar{r} = 20.$, $\bar{\epsilon}_1 = 2.34$, $\bar{\epsilon}_2 = 2.25$, $\bar{\epsilon}_3 = 1.0$.

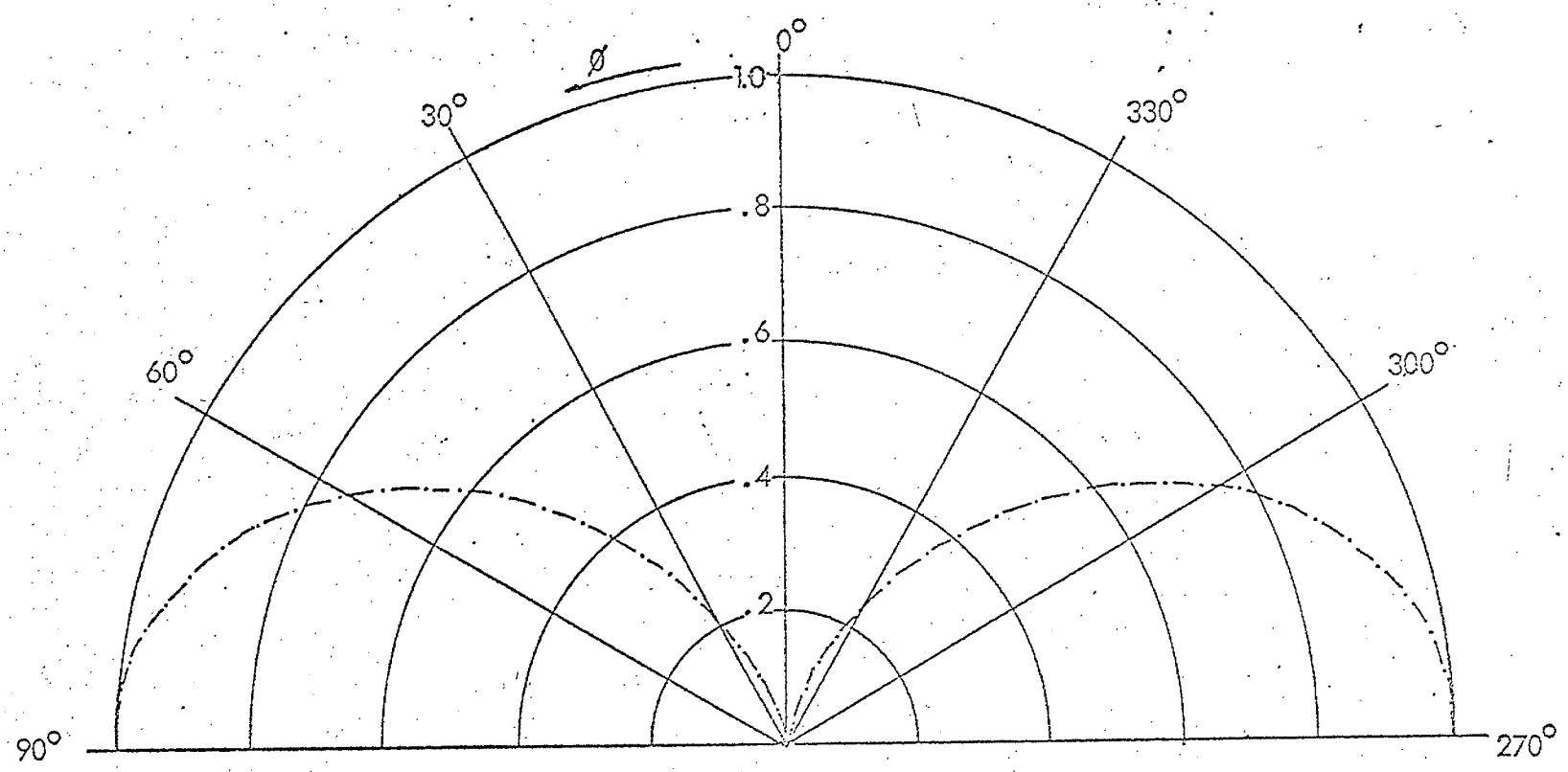

FIGURE 3.c Radiation Power Pattern $P(90^\circ, \phi)$:

— · — · — · V = 0.1, 1.5, 2.4.

As stated before, the power radiated by a small scattering volume on the fiber axis is given by

$$P_r = 1/2 \; I_m^2 \; R_r \tag{3.8}$$

$$= 1/2 \, (\omega \, \Delta\epsilon \; | \, E_i' \; | \, A_1 \; V')^2 \; R_r, \text{ for a dielectric particle } (\epsilon')$$

Taking the ratio of P_r to P_i and normalizing with scattering parameters $(\Delta\epsilon \, , \, v')$, we finally get

$$\frac{P_r}{P_i \, (\Delta\bar{\epsilon} \, \bar{v}')^2} = \frac{c^4}{2\pi Z_o^2} \cdot \frac{V^2}{(\bar{\epsilon}_1 - \bar{\epsilon}_2)} \cdot \frac{|E_i'|^2}{\bar{S}_i(V)} \, \bar{R}_r(V) \tag{3.9}$$

where $\Delta\bar{\epsilon} = (\bar{\epsilon}' - \bar{\epsilon})$, $\bar{\epsilon}'$ - scattering particle

$\bar{v}' = \dfrac{v'}{a^3}$, normalized scattering volume (a is core radius of fibre)

$$Z_o = \sqrt{\frac{\mu_o}{\epsilon_o}} = 376.7 \; \Omega$$

$$c = \frac{a}{b} = \frac{\text{(core radius)}}{\text{(cladding radius)}}$$

$|E_i'|$ = transverse field intensity at the scattering centre

$\bar{R}_r(V) = b^2 R_r$, normalized radiation resistance for a point source on the fibre axis

For the infinite medium approximation (with a refractive index $n_1 = \sqrt{\epsilon_1}$), we merely replace the normalized radiation resistance $(\bar{R}_1)$ of the cladded fibre by the corresponding one of the infinite medium, i.e.,

$$\bar{R}_r(V) \rightarrow [b^2 R_o] \tag{3.10}$$

where $R_o = \left(\frac{80\pi^2}{n_1}\right) \cdot \left(\frac{1}{\lambda_o^2}\right)$, radiation resistance of a point source in an infinite medium (n_1)

In Figure 4, we plot the fraction of power scattered into radiation normalized according to equation (3.9). The infinite medium approximation is also shown for comparison. We conclude from the results that the infinite medium approximation is reasonably good and may disagree by about one or two dB with the exact solution. This is for a scattering centre on or very near the fibre axis. It is speculated, however, that an off-axis scattering centre might produce a more pronounced difference.

The ratio of the exact solution of the power radiated (P_r) to the infinite-medium approximation (P_o) is given by

$$\frac{P_r}{P_o} = \frac{\frac{1}{2} I_m R_r}{\frac{1}{2} I_m R_o} = \frac{R_r}{R_o} \tag{3.11}$$

which is just the ratio of the corresponding radiation resistances as defined earlier.

The variation of this ratio with the permittivity difference between the core and cladding, i.e., $\Delta\bar{\epsilon} = (\bar{\epsilon}_1 - \bar{\epsilon}_2)$, is illustrated in Figure 5. Contrary to the expected result of having the ratio approach one as the difference $\Delta\bar{\epsilon}$ goes to zero, the graph shows an oscillatory behaviour about the value one. The departure illustrates the difference between the exact solution and the infinite-medium approximation.

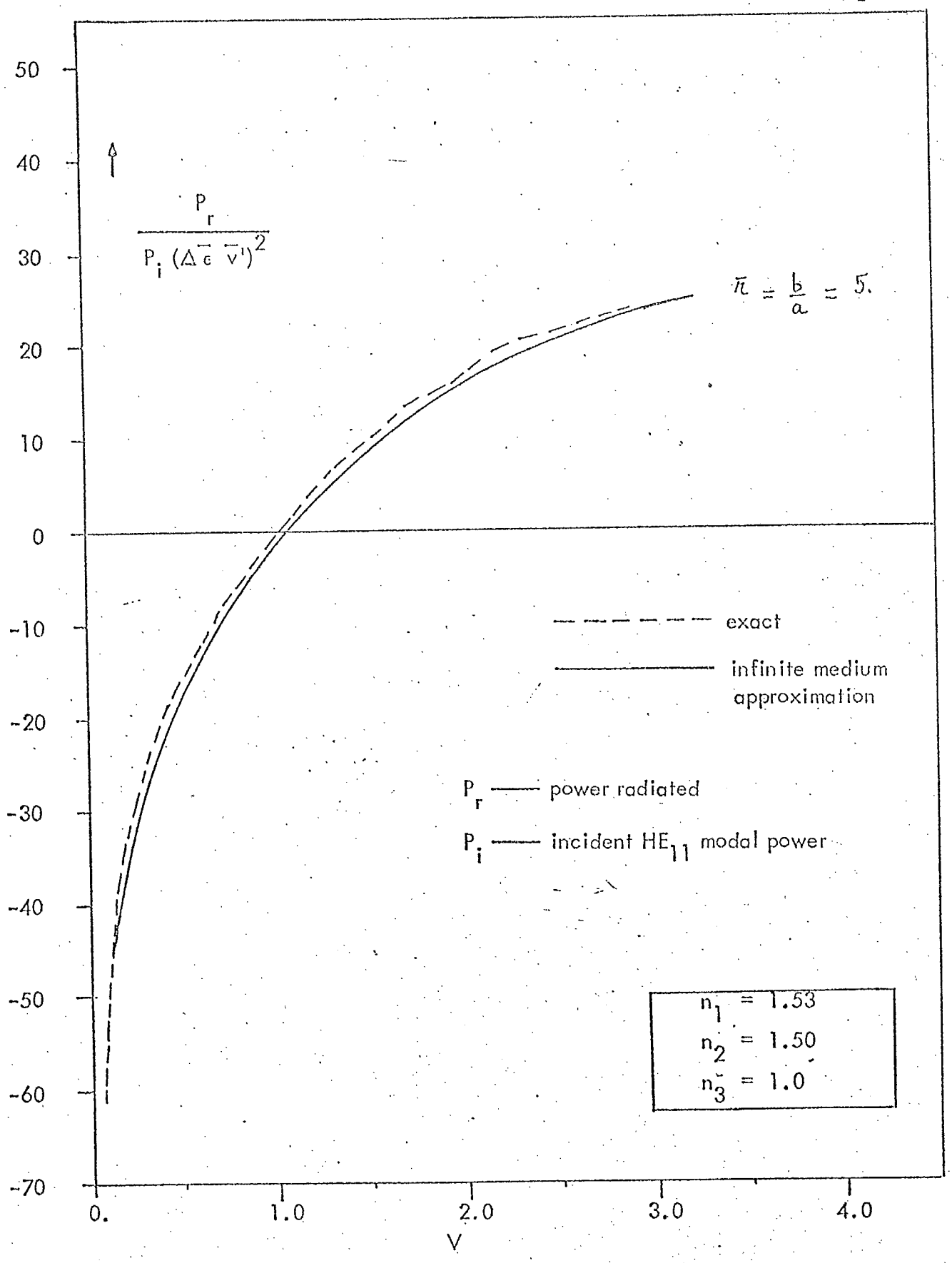

FIGURE 4.a Power Radiated from a Scattering Particle $(\bar{\epsilon}, \bar{v}')$ on the Fibre Axis.

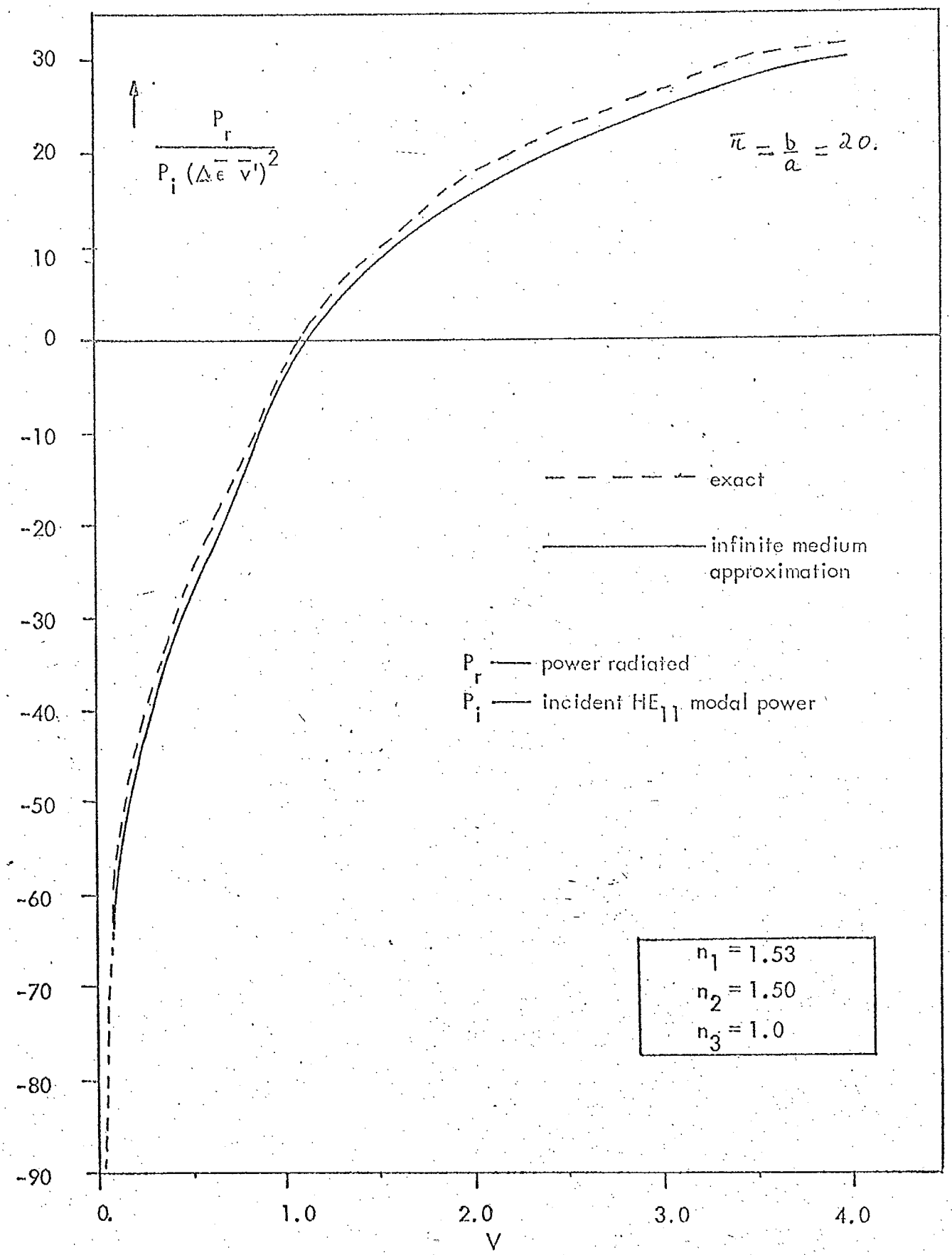

FIGURE 4.b Power Radiated from a Scattering Particle $(\bar{\epsilon}, \bar{v}')$ on the Fibre Axis.

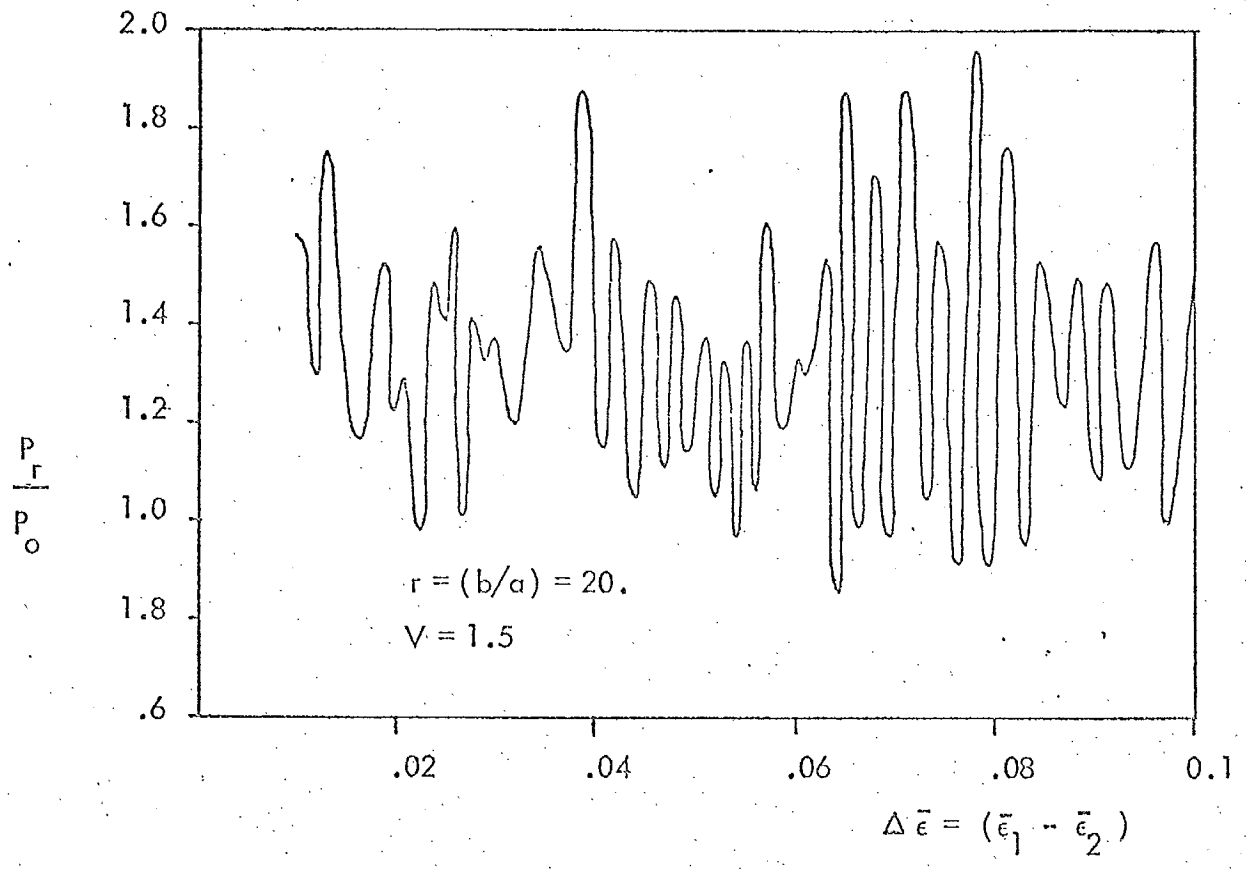

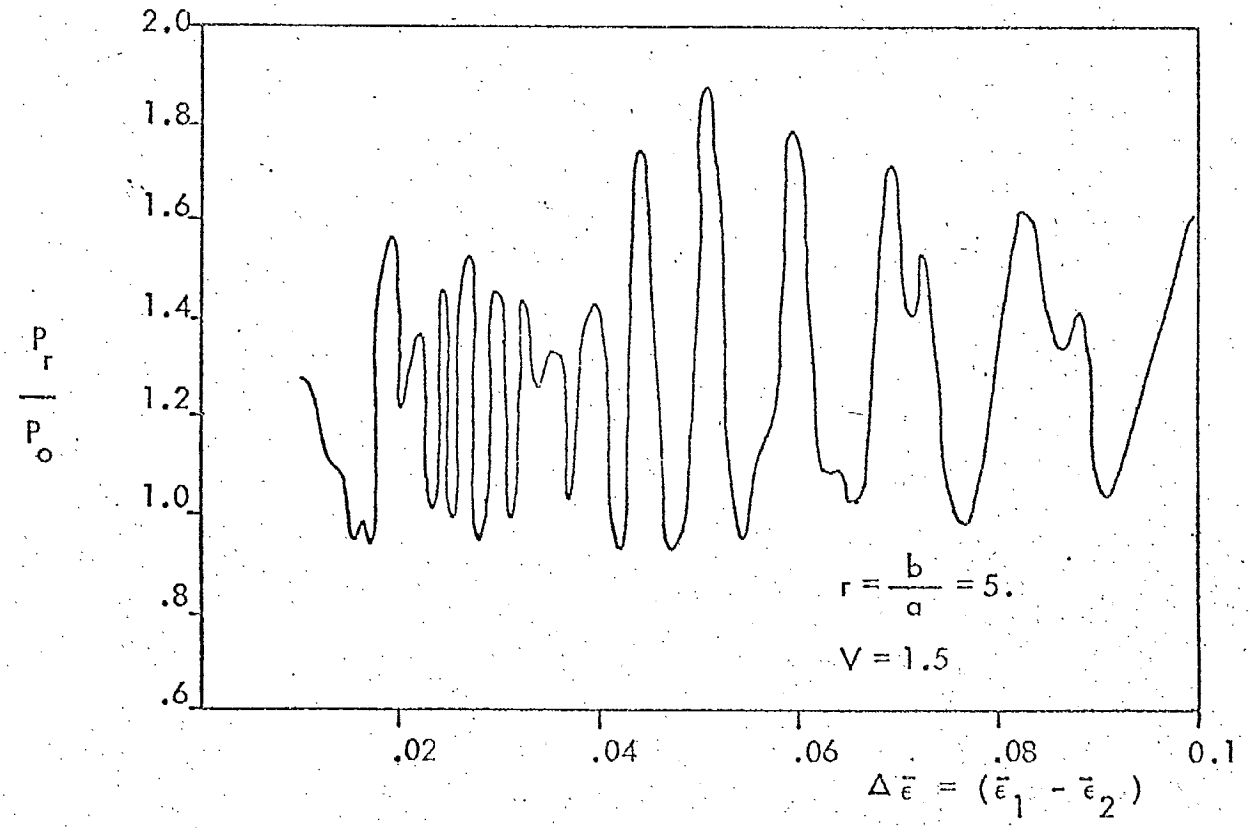

FIG. 5 Normalized radiated power $\left(\frac{P_r}{P_o}\right)$ versus dielectric difference $\Delta\bar{\epsilon}$, where $\bar{\epsilon}_1 = 2.34$, $\bar{\epsilon}_2$ varied, $\bar{\epsilon}_3 = 1.0$.

A letter which reported some preliminary results on the problem of scattering loss from a localized inhomogeneity in a cladded optical fiber has been published and is included herewith.

Fig. 5 should replace Fig. 2 in the letter.

SCATTERING LOSS IN A CLADDED-FIBRE OPTICAL WAVEGUIDE

Indexing terms: Optical waveguides, Fibre optics, Light Scattering, Green's-function methods

An exact analysis using the Green's-function formulation of the problem of scattering from a local inhomogeneity inside a cladded-fibre waveguide is carried out, and yields a radiation loss higher than that evaluated from the infinite-medium approximation

There is considerable current interest in improving the transmission characteristics of glass-fibre optical waveguides, and one specific problem in this domain is the reduction of the attenuation of the optical waves caused by losses in a cladded fibre. Such losses arise because of both absorption and scattering.[1-3] The absorption is caused by traces of metallic ions in the glass fibre. Scattering losses are mainly caused by Rayleigh scattering and scattering due to imperfections in the bulk of the core and in the 'waveguide' imperfections. The former is due to minute dielectric inhomogeneities frozen in the glass, while the latter may be introduced by such fabrication-induced scatterers as bubbles, crystallites, dust particles, cracks, core-cladding irregularities etc. The presence of scattering centres causes loss of energy by radiation when light is guided by the fibre. Further, power carried in the guided mode (the dominant HE_{11} mode in a monomode fibre) is scattered also into higher-order modes. This mode-conversion and reconversion phenomenon causes error signals, and limits the channel capacity in an optical-communication system.

The object of this letter is to present a theoretical model to account for losses due to discrete scattering centres within the cladded fibre. For the present purpose, the discussion is confined to a consideration of the radiation loss from one scattering centre in a single-mode cladded fibre operating in the dominant HE_{11} mode. It is assumed that the scatterer is small compared with the incident wavelength and the size of the fibre, conditions that are usually met in practice. To a first approximation, the scatterer can be assumed to be approximately spherical in shape, and hence Rayleigh theory[4] holds. It thus follows that the radiation fields from the spherical scatterer are the same as those from a short electric dipole parallel to the incident electric field and with a dipole moment

$$\tilde{P} = 4\pi\varepsilon_0\,\varepsilon_2\,\frac{N^2-1}{N^2+2}\,r^3\,\tilde{E}_i \qquad (1)$$

where

$$N^2 = \frac{\varepsilon_1'}{\varepsilon_1} + j\frac{\sigma_1'}{\omega\varepsilon_0\,\varepsilon_1} = \left(\frac{n_1'}{n_1}\right)^2 \qquad (2)$$

and n_1' and n_1 are the refractive indices of the scatterer and the surrounding medium, respectively. $\varepsilon_0\,\varepsilon_1'$ and σ_1' are the permittivity and conductivity of the scatterer, $\varepsilon_0\,\varepsilon_1$ is the permittivity of the surrounding medium, r is the radius of the scattering sphere and $\tilde{E}_i$ is the amplitude of the incident electric field. Hence the current moment of the short dipole is related to the dipole moment by

$$I\Delta x = j\omega\tilde{P} \qquad (3)$$

where Δx is the length of the dipole and ω is the angular frequency of the incident wave. The current moment can also be expressed as $\tilde{J}\Delta v$, where J is the induced current density in the scatterer and Δv is its volume. Snyder,[1] and Clarricoats and Chan[3] considered the problem of radiation loss from a scattering centre in a cladded fibre by assuming the cladding to be infinite in extent, and, because of the small dielectric difference between the core and the cladding, using the expression for the power radiated from an infinitesimal dipole into an infinite medium $\varepsilon_0\,\varepsilon_1$

$$P_r = \frac{\pi}{3}\left(\sqrt{\mu_0\,\varepsilon_0\,\varepsilon_1}\right)\left(\frac{\Delta v\,|\tilde{J}|^2}{\lambda}\right) \qquad (4)$$

as an approximation. It was pointed out by these authors that the Green's-function formulation for open-bounded cylindrical hybrid-mode structures is extremely complex. However, for the simpler case of a transversely oriented infinitesimal dipole on the axis of a dielectric rod, the Green's function is available. We shall now extend the analysis[5] developed previously for a dielectric rod to a cladded fibre. The method of analysis involves expressing the dipole and the fields as a Fourier integral in the z direction and a Fourier series in the

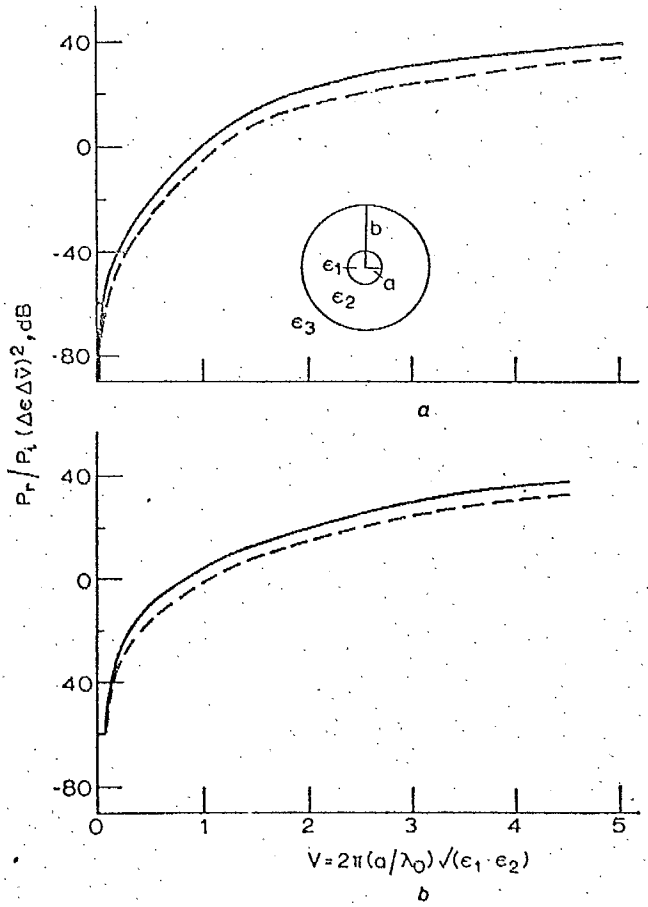

Fig. 1 *Normalised radiated power $P_r/P_i(\Delta\varepsilon\Delta v)^2$ against the normalised frequency $V = 2\pi(a/\lambda_0)\sqrt{(\varepsilon_1-\varepsilon_2)}$*

P_i is the power in the incident HE_{11} mode
$\Delta\varepsilon$ $\varepsilon_1-\varepsilon_1'$
Δv $\Delta v/r^3$
Dielectric ε_1
——— exact
– – – – infinite medium
(a) $b/a = 20$, $\varepsilon_1 = 2{\cdot}34$, $\varepsilon_2 = 2{\cdot}25$, $\varepsilon_3 = 1{\cdot}0$
(b) $b/a = 5$, $\varepsilon_1 = 2{\cdot}34$, $\varepsilon_2 = 2{\cdot}25$, $\varepsilon_3 = 1{\cdot}0$

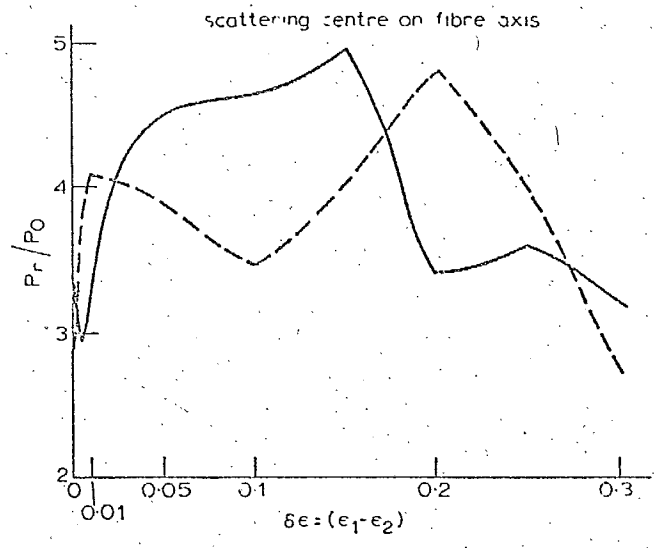

Fig. 2 *Normalised radiated power P_r/P_0 against dielectric difference $\delta\varepsilon$*

$P_0 = \frac{J_x^2}{2}\left(\frac{80\pi^2}{\sqrt{\varepsilon_1}}\right)\left(\frac{1}{\lambda_0^2}\right)$
$V = 2{\cdot}405$
$\varepsilon_1 = 2{\cdot}34$, ε_2 varied, $\varepsilon_3 = 1{\cdot}0$
——— $b/a = 20$
– – – – $b/a = 5$

ϕ direction in a cylindrical co-ordinate system. The longitudinal components of the fields are given, in the core $(0 < \rho < a)$, by

$$\left.\begin{aligned} jE_{z1,m}(\rho,\gamma) &= \bar{J}_e \eta_1 \left\{ \frac{j}{2} \frac{\gamma}{\varepsilon_1} Y_1(k_0 \eta_1 \rho) + A_m(\gamma) J_1(k_0 \eta_1 \rho) \right\} \\ H_{z1,m}(\rho,\gamma) &= \bar{J}_e \eta_1 \left\{ -\frac{j}{2} Y_1(k_0 \eta_1 \rho) + B_m(\gamma) J_1(k_0 \eta_1 \rho) \right\} \end{aligned}\right\} \quad (5)$$

in the cladding $(a < \rho < b)$, by

$$\left.\begin{aligned} jE_{z2,m}(\rho,\gamma) &= \bar{J}_e \eta_2 \{E_m(\gamma) Y_1(k_0 \eta_2 \rho) + F_m(\gamma) J_1(k_0 \eta_2 \rho)\} \\ H_{z2,m}(\rho,\gamma) &= \bar{J}_e \eta_2 \{C_m(\gamma) Y_1(k_0 \eta_2 \rho) + D_m(\gamma) J_1(k_0 \eta_2 \rho)\} \end{aligned}\right\} \quad (6)$$

and, in the free space $(\rho > b)$, by

$$\left.\begin{aligned} jE_{z3,m}(\rho,\gamma) &= \bar{J}_e L_m(\gamma) H_1^{(1)}(k_0 \eta_0 \rho) \\ H_{z3,m}(\rho,\gamma) &= \bar{J}_e G_m(\gamma) H_1^{(1)}(k_0 \eta_0 \rho) \end{aligned}\right\} \quad (7)$$

where

$$\bar{J}_e = j \frac{J_e}{4} k_0 \sqrt{\mu_0}$$

$m = 1$ or -1, $\eta_1 = \sqrt{(\varepsilon_1 - \gamma^2)}$, $\eta_2 = \sqrt{(\varepsilon_2 - \gamma^2)}$, $\eta_0 = \sqrt{(1 - \gamma^2)}$, J_e is the current moment on the dipole and γ is the Fourier transform variable, and G_m and L_m are two of the eight unknown coefficients in the fields that can be determined through the imposition of boundary conditions. On applying the Fourier transformation and Parseval's theorem, the total radiated power is given by

$$P_r = \frac{J_e^2}{2} \left(\sqrt{\frac{\mu_0}{\varepsilon_0}} \right) \frac{k_0^2}{4\pi} \sum_{m=1,-1} \int_0^1 \left(\left| \frac{G_m}{\eta_0} \right|^2 + \left| \frac{L_m}{\eta_0} \right|^2 \right) d\gamma \quad (8)$$

and can be evaluated by numerical integration. Fig. 1 presents results of $P_r/P_i(\Delta\varepsilon\Delta\bar{v})^2$ as a function of the normalised frequency $V = 2\pi(a/\lambda_0)\sqrt{(\varepsilon_1 - \varepsilon_2)}$ for two different values of a/b, where P_i is the incident power in the HE_{11} mode, $\delta\varepsilon = \varepsilon_1 - \varepsilon_2$ and $\Delta\bar{v} = \Delta v/r^3$. It is interesting to note that the radiation loss calculated from the Green's-function solution is about 5 dB higher than that obtained by the infinite-medium approximation of eqn. 4. Within the validity of the Rayleigh theory, the Green's-function solution gives the exact solution where boundary effects at core-cladding and cladding–free-space interfaces have been taken into account, and hence against which the accuracy of approximate solutions can be checked. The 5 dB is the difference in the calculated power radiated when only one scattering centre is considered. In a long fibre, there will be many scattering centres, and the cumulative difference in the calculated transmitted power levels over a certain distance of the fibre can, therefore, be quite appreciable.

In Fig. 2, the ratio P_r/P_0 has been plotted as a function of the dielectric difference, where P_0 is the power radiated from the same dipole into an infinite medium ε_1, as given by eqn. 4. This ratio does not approach unity as the dielectric difference vanishes $(\delta\varepsilon \to 0)$, because, in the present treatment, the finite boundary at $\rho = b$ has been taken into account, so that, in the limit, the cladded fibre becomes a dielectric rod as $\delta\varepsilon$ approaches zero. The variations observed in the calculated power with changes in $\delta\varepsilon$ illustrate the departure from the infinite-ε_1-medium approximation when the boundary effects are taken into account.

To summarise, we see that the infinite-medium approximation in the evaluation of radiated power from a scattering centre can lead to inaccuracies. Within the validity of the Rayleigh scattering theory, the Green's-function formulation yields the exact solution. Moreover, the latter method can also be used to compute the spatial distribution of scattered power. This result, as well as other pertinent data, will be reported later.

Acknowledgment: The work reported here is supported by the Communications Research Centre, Ottawa, Canada, and also the National Research Council of Canada. A helpful discussion with A. W. Snyder is acknowledged.

G. L. YIP
J. MARTUCCI
G. W. FARNELL

Department of Electrical Engineering
McGill University
PO Box 6070, Montreal 101, Que., Canada

1st June 1973

References

1 SNYDER, A. W.: 'Excitation and scattering of modes on a dielectric or optical fiber', *IEEE Trans.*, 1969, MTT-17, p. 1138
2 TYNES, A. R., PEARSON, A. D., and BISHEE, D. L.: 'Loss mechanisms and measurements in clad glass fibers and bulk glass', *J. Opt. Soc. Am.*, 1971, 61, p. 143
3 CHAN, K. B.: 'Electromagnetic wave propagation in optical waveguides', Ph.D. dissertation, University of London, 1972
4 VAN DE HULST, H. C.: 'Light scattering by small particles' (Wiley, 1957)
5 YIP, G. L.: 'Launching efficiency of the HE_{11} surface wave mode on a dielectric rod', *IEEE Trans.*, 1970, MTT-18, p. 1034

4. Surface-Wave Power

For $z > 0$, the surface wave contribution to the fields, e.g., $H_{z3}(\rho, \varphi, z)$ and $i E_{z3}(\rho, \varphi, z)$ can be obtained by evaluating the residues at the poles $\gamma = \gamma_s$ with the following results.

For $0 < \rho < a$:

$$H_{z1}(\rho,\phi,z) = i K_0 J_e \sum_{m=\pm 1} \frac{\bar{B}_m(\gamma)}{\Delta'(\gamma_s)} \eta_1 J_1(K_0 \eta_1 \rho) e^{im\phi} e^{iK_0\gamma_s z}$$

$$i E_{z1}(\rho,\phi,z) = i K_0 J_e \sum_{m=\pm 1} \frac{\bar{A}_m(\gamma)}{\Delta'(\gamma_s)} \eta_1 J_1(K_0 \eta_1 \rho) e^{im\phi} e^{iK_0\gamma_s z} \tag{4.1}$$

where $\Delta'(\gamma_s) = \left.\dfrac{\partial \Delta(\gamma)}{\partial \gamma}\right|_{\gamma = \gamma_s}$

For $a < \rho < b$:

Case 1: When both η_1 and η_2 are real ("Leaky" modes)

$$H_{z2}(\rho,\phi,z) = i K_0 J_e \sum_{m=\pm 1} \frac{[\bar{C}_m Y_1(K_0\eta_2\rho) + \bar{D}_m J_1(K_0\eta_2\rho)]}{\Delta'(\gamma_s)} e^{im\phi} e^{iK_0\gamma_s z} \tag{4.2a}$$

$$i E_{z2}(\rho,\phi,z) = i K_0 J_e \sum_{m=\pm 1} \frac{[\bar{E}_m Y_1(K_0\eta_2\rho) + \bar{F}_m J_1(K_0\eta_2\rho)]}{\Delta'(\gamma_s)} e^{im\phi} e^{iK_0\gamma_s z}$$

Case 2: When η_1 real and η_2 imaginary ("propagating" modes)

$$H_{z2}(\rho,\phi,z) = iK_0 J_e \sum_{m=\pm 1} \frac{[\bar{C}_m' K_1(K_0|\eta_2|\rho) + \bar{D}_m' I_1(K_0|\eta_2|\rho)]}{\Delta'(\gamma_s)} e^{im\phi} e^{iK_0\gamma_s z}$$

$$iE_{z2}(\rho,\phi,z) = iK_0 J_e \sum_{m=\pm 1} \frac{[\bar{E}_m' K_1(K_0|\eta_2|\rho) + \bar{F}_m' I_1(K_0|\eta_2|\rho)]}{\Delta'(\gamma_s)} e^{im\phi} e^{iK_0\gamma_s z} \tag{4.2b}$$

For $\rho > b$

$$H_{z3}(\rho,\phi,z) = -i|\eta_0| J_e \sum_{m=\pm 1} \frac{2}{\pi} \frac{\bar{G}_m K_1(K_0|\eta_0|\rho)}{\Delta'(\gamma_s)} e^{im\phi} e^{iK_0\gamma_s z}$$

$$iE_{z3}(\rho,\phi,z) = -i|\eta_0| J_e \sum_{m=\pm 1} \frac{2}{\pi} \frac{I_m K_1(K_0|\eta_0|\rho)}{\Delta'(\gamma_s)} e^{im\phi} e^{iK_0\gamma_s z} \tag{4.3}$$

Other field components can also be obtained by the use of Eq. (2.5).

Because of symmetry, the total power carried by surface waves is twice that in the positive z direction.

$$P_s = 2\,P_{s+} = 2\,(P_{s1} + P_{s2} + P_{s3}) \tag{4.4}$$

where

$$P_{s1} = \frac{1}{2\sqrt{\mu_0 \epsilon_0}} \mathrm{Re} \int_0^{2\pi}\int_0^a \rho\, d\rho\, d\phi \left\{ E_{\rho 1}(\rho,\phi,z) H_{\phi 1}^*(\rho,\phi,z) - E_{\phi 1}(\rho,\phi,z) H_{\rho 1}^*(\rho,\phi,z) \right\} \tag{4.5a}$$

$$P_{s2} = \frac{1}{2\sqrt{\mu_o \epsilon_o}} \, Re \int_0^{2\pi}\int_a^b \rho \, d\rho \, d\phi \left\{ E_{\rho 2}(\rho,\phi,z) H^*_{\phi 2}(\rho,\phi,z) - E_{\phi 2}(\rho,\phi,z) H^*_{\rho 2}(\rho,\phi,z) \right\} \tag{4.5b}$$

$$P_{s3} = \frac{1}{2\sqrt{\mu_o \epsilon_o}} \, Re \int_0^{2\pi}\int_b^{\infty} \rho \, d\rho \, d\phi \left\{ E_{\rho 3}(\rho,\phi,z) H^*_{\phi 3}(\rho,\phi,z) - E_{\phi 3}(\rho,\phi,z) H^*_{\rho 3}(\rho,\phi,z) \right\} \tag{4.5c}$$

Thus,

$$P_{s1} = \frac{\pi}{\sqrt{\mu_o \epsilon_o}} \, Re \int_0^{a} \rho \, d\rho \sum_{m=\pm 1} \left\{ E_{\rho 1,m}(\rho) H^*_{\phi 1,m}(\rho) - E_{\phi 1,m}(\rho) H^*_{\rho 1,m}(\rho) \right\} \tag{4.6a}$$

$$P_{s2} = \frac{\pi}{\sqrt{\mu_o \epsilon_o}} \, Re \int_a^{b} \rho \, d\rho \sum_{m=\pm 1} \left\{ E_{\rho 2,m}(\rho) H^*_{\phi 2,m}(\rho) - E_{\phi 2,m}(\rho) H^*_{\rho 2,m}(\rho) \right\} \tag{4.6b}$$

$$P_{s3} = \frac{\pi}{\sqrt{\mu_o \epsilon_o}} \, Re \int_b^{\infty} \rho \, d\rho \sum_{m=\pm 1} \left\{ E_{\rho 3,m}(\rho) H^*_{\phi 3,m}(\rho) - E_{\phi 3,m}(\rho) H^*_{\rho 3,m}(\rho) \right\} \tag{4.6c}$$

It is clear from above expressions that total surface-wave power is equal to the summation of power carried by the individual modes, and there is no contribution from the cross-over terms.

Finally, from eqs. (2.5), (4.1), (4.2), (4.3), and (4.6), we have

$$P_{s1} = \left(\frac{J_e^2}{2}\right)\frac{15\pi^2}{4|\Delta'(\gamma_s)|^2} K_o^4 a^2 J_1^2(K_o\eta_1 a)\, Re\left\{\left(\frac{J_o^2(K_o\eta_1 a)}{J_1^2(K_o\eta_1 a)}+1\right)\sum_{m=\pm1} Q_{3,m} - \frac{4}{K_o^2\eta_1^2 a^2}\sum_{m=\pm1} Q_{2,m}\right\} \tag{4.7}$$

where $Q_{3,m} = 2\gamma(\epsilon_1|\bar{A}_m|^2 + |\bar{B}_m|^2)$

$$Q_{2,m} = \gamma(\epsilon_1|\bar{A}_m|^2 + |\bar{B}_m|^2) + m(\gamma^2\bar{A}_m\bar{B}_m^* + \epsilon_1\bar{A}_m^*\bar{B}_m)$$

For case 1, when both η_1 and η_2 are real

$$P_{s2} = I_1 + I_2 + I_3$$

where

$$I_1 = \left(\frac{J_e^2}{2}\right)\frac{15\pi^2}{4|\Delta'(\gamma_s)|^2} K_o^4 b^2 Y_1^2(K_o\eta_2 b)\, Re\left\{\left(\frac{Y_o^2(K_o\eta_2 b)}{Y_1^2(K_o\eta_2 b)}+1\right)\sum_{m=\pm1} Q_{23,m} - \frac{4}{K_o^2\eta_2^2 b^2}\sum_{m=\pm1} Q_{22,m}\right\}$$

$$-\left(\frac{J_e^2}{2}\right)\frac{15\pi^2}{4|\Delta'(\gamma_s)^2} K_o^4 a^2 Y_1^2(K_o\eta_2 a)\, Re\left\{\left(\frac{Y_o^2(K_o\eta_2 a)}{Y_1^2(K_o\eta_2 a)}+1\right)\sum_{m=\pm1} Q_{23,m} - \frac{4}{K_o^2\eta_2^2 a^2}\sum_{m=\pm1} Q_{22,m}\right\} \tag{4.8a}$$

$$I_2 = \left(\frac{J_e^2}{2}\right)\frac{15\pi^2}{4|\Delta'(\gamma_s)|^2} K_o^4 b^2 J_1^2(K_o\eta_2 b)\ Re\left\{\left(\frac{J_o^2(K_o\eta_2 b)}{J_1^2(K_o\eta_2 b)}+1\right)\sum_{m=\pm1} Q_{26,m} - \frac{4}{K_o^2\eta_2^2 b^2}\sum_{m=\pm1} Q_{25,m}\right\}$$

$$-\left(\frac{J_e^2}{2}\right)\frac{15\pi^2}{4|\Delta'(\gamma_s)|^2} K_o^4 a^2 J_1^2(K_o\eta_2 a)\ Re\left\{\left(\frac{J_o^2(K_o\eta_2 a)}{J_1^2(K_o\eta_2 a)}+1\right)\sum_{m=\pm1} Q_{26,m} - \frac{4}{K_o^2\eta_2^2 a^2}\sum_{m=\pm1} Q_{25,m}\right\} \tag{4.8b}$$

$$I_3 = \frac{15\pi^2}{|\Delta'(\gamma_s)|^2\eta_2^2} K_o^2\ Re\left\{\frac{K_o^2\eta_2^2 b^2}{2} S_5 \sum_{m=\pm1} D_1 + S_4 \sum_{m=\pm1}(D_1+D_2)\right\} \tag{4.8c}$$

$$Q_{23,m} = 2\gamma(|\bar{C}_m|^2 + \epsilon_2|\bar{E}_m|^2)$$

$$Q_{22,m} = \gamma(|\bar{C}_m|^2 + \epsilon_2|\bar{E}_m|^2) + m(\gamma^2\bar{C}_m^*\bar{E}_m + \epsilon_2\bar{C}_m\bar{E}_m^*)$$

$$Q_{26,m} = 2\gamma(|\bar{D}_m|^2 + \epsilon_2|\bar{F}_m|^2)$$

$$Q_{25,m} = \gamma(|\bar{D}_m|^2 + \epsilon_2|\bar{F}_m|^2) + m(\gamma^2\bar{D}_m^*\bar{F}_m + \epsilon_2\bar{D}_m\bar{F}_m^*)$$

$$S_4 = J_1(K_o\eta_2 a)Y_1(K_o\eta_2 a) - J_1(K_o\eta_2 b)Y_1(K_o\eta_2 b)$$

$$S_5 = [J_o(K_o\eta_2 b)Y_o(K_o\eta_2 b) + J_1(K_o\eta_2 b)Y_1(K_o\eta_2 b)] - c^2[J_o(K_o\eta_2 a)Y_o(K_o\eta_2 a) + J_1(K_o\eta_2 a)Y_1(K_o\eta_2 a)]$$

$$D_1 = \gamma[(\bar{C}_m\bar{D}_m^* + \bar{C}_m^*\bar{D}_m) + \epsilon_2(\bar{E}_m\bar{F}_m^* + \bar{E}_m^*\bar{F}_m)]$$

$$D_2 = m[\gamma^2(\bar{C}_m^*\bar{F}_m + \bar{D}_m\bar{E}_m) + \epsilon_2(\bar{C}_m\bar{F}_m^* + \bar{D}_m\bar{E}_m^*)]$$

For case 2, when η_1 real and η_2 imaginary:

$$P_{s2} = L_1 + L_2 + L_3$$

where

$$L_1 = \left(\frac{J_e^2}{2}\right)\frac{15\pi^2}{4|\Delta'(\gamma_5)|^2} K_0^4 b^2 K_1^2(K_0|\eta_2|b)\, Re\left\{\left(\frac{K_0^2(K_0|\eta_2|b)}{K_1^2(K_0|\eta_2|b)} - 1\right)\sum_{m=\pm1} Q'_{23,m} - \frac{4}{K_0^2|\eta_2|^2 b^2}\sum_{m=\pm1} Q'_{22,m}\right\}$$

$$-\left(\frac{J_e^2}{2}\right)\frac{15\pi^2}{4|\Delta'(\gamma_5)|^2} K_0^4 a^2 K_1^2(K_0|\eta_2|a)\, Re\left\{\left(\frac{K_0^2(K_0|\eta_2|a)}{K_1^2(K_0|\eta_2|a)} - 1\right)\sum_{m=\pm1} Q'_{23,m} - \frac{4}{K_0^2|\eta_2|^2 a^2}\sum_{m=\pm1} Q'_{22,m}\right\} \tag{4.9a}$$

$$L_2 = \left(\frac{J_e^2}{2}\right)\frac{15\pi^2}{4|\Delta'(\gamma_5)|^2} K_0^4 b^2 I_1^2(K_0|\eta_2|b)\, Re\left\{\left(\frac{I_0^2(K_0|\eta_2|b)}{I_1^2(K_0|\eta_2|b)} - 1\right)\sum_{m=\pm1} Q'_{26,m} - \frac{4}{K_0^2|\eta_2|^2 b^2}\sum_{m=\pm1} Q'_{25,m}\right\}$$

$$-\left(\frac{J_e^2}{2}\right)\frac{15\pi^2}{4|\Delta'(\gamma_5)|^2} K_0^4 a^2 I_1^2(K_0|\eta_2|a)\, Re\left\{\left(\frac{I_0^2(K_0|\eta_2|a)}{I_1^2(K_0|\eta_2|a)} - 1\right)\sum_{m=\pm1} Q'_{26,m} - \frac{4}{K_0^2|\eta_2|^2 a^2}\sum_{m=\pm1} Q'_{25,m}\right\} \tag{4.9b}$$

$$L_3 = \left(\frac{J_e^2}{2}\right)\frac{15\pi^2}{|\Delta'(\gamma_5)|^2|\eta_2|^2} K_0^2\, Re\left\{-\frac{K_0^2|\eta_2|^2 b^2}{2} S'_5 \sum_{m=\pm1} D'_1 + S'_4 \sum_{m=\pm1}(D'_1 + D'_2)\right\} \tag{4.9c}$$

$$Q'_{23,m} = 2\gamma(|\bar{C}'_m|^2 + \epsilon_2|\bar{E}'_m|^2)$$

$$Q'_{22,m} = \gamma(|\bar{C}'_m|^2 + \epsilon_2|\bar{E}'_m|^2) + m(\gamma^2 \bar{C}'^*_m \bar{E}'_m + \epsilon_2 \bar{C}'_m \bar{E}'^*_m)$$

$$Q'_{26,m} = 2\gamma(|\bar{D}'_m|^2 + \epsilon_2|\bar{F}'_m|^2)$$

$$Q'_{25,m} = \gamma(|\bar{D}'_m|^2 + \epsilon_2|\bar{F}'_m|^2) + m(\gamma^2 \bar{D}'^*_m \bar{F}'_m + \epsilon_2 \bar{D}'_m \bar{F}'^*_m)$$

$$S'_4 = -I_1(K_0|\eta_2|b)K_1(K_0|\eta_2|b) + I_1(K_0|\eta_2|a)K_1(K_0|\eta_2|a)$$

$$S'_5 = -[I_0(K_0|\eta_2|b)K_0(K_0|\eta_2|b) + I_1(K_0|\eta_2|b)K_1(K_0|\eta_2|b)] + c^2[I_0(K_0|\eta_2|a)K_0(K_0|\eta_2|a) + I_1(K_0|\eta_2|a)K_1(K_0|\eta_2|a)]$$

$$D_1' = \gamma\left[(\bar{C}_m'^{*}\bar{D}_m' + \bar{C}_m'\bar{D}_m'^{*}) + \epsilon_2(\bar{E}_m'\bar{F}_m'^{*} + \bar{E}_m'^{*}\bar{F}_m')\right]$$

$$D_2' = m\left[\gamma^2(\bar{C}_m'^{*}\bar{F}_m' + \bar{D}_m'^{*}\bar{E}_m') + \epsilon_2(\bar{C}_m'\bar{F}_m'^{*} + \bar{D}_m'\bar{E}_m'^{*})\right]$$

Finally,

$$P_{s3} = \left(\frac{J_e^2}{2}\right)\frac{15\pi^2}{|\Delta'(\gamma_s)|^2} k_o^4 b^2 K_1^2(k_o|\eta_o|b)\, \mathrm{Re}\left\{\left(1 - \frac{K_o^2(k_o|\eta_o|b)}{K_1^2(k_o|\eta_o|b)}\right)\sum_{m=\pm 1} Q_{33,m} + \frac{4}{k_o^2|\eta_o|^2 b^2}\sum_{m=\pm 1} Q_{32,m}\right\} \tag{4.10}$$

$$Q_{33,m} = 2\gamma(|\bar{I}_m|^2 + |\bar{G}_m|^2)$$

$$Q_{32,m} = \left[\gamma(|\bar{I}_m|^2 + |\bar{G}_m|^2) + m(\gamma^2\bar{I}_m\bar{G}_m^{*} + \bar{I}_m^{*}\bar{G}_m)\right]$$

And the total surface wave powers can be normalized with respect to the source current according to

$$P_s = \frac{J_e^2}{2}\,\bar{P}_s \tag{4.11}$$

where $\bar{P}_s$ is the normalized power.

5. Results and Discussions on Mode Conversion due to a Scattering Center

First the surface-wave power expressions are checked with those of the rod case by making $\bar{\epsilon}_2 = 1.001$ and $C = 0.9999$. It is found under this specified situation, the surface wave power agrees very well with that of the rod case. This checks the correctness of the analysis.

Fig. 6 shows the computed results of $\bar{P}_s$ for HE_{11}, EH_{11}, and HE_{12} versus the normalized frequency V. At the transition from the cladding (leaky) modes to the core (propagating) modes, $\bar{P}_s$ goes through some kind of a minimum. From the characteristic curves in Fig. 2, the transition from the cladding region to the core region of the HE_{11} mode is sharp, hence the transition of $\bar{P}_s$ from the cladding region to the core region is sharp too. For the EH_{11} and HE_{12} modes, the transition is wide over a band of normalized frequency, hence also wide is the transition of $\bar{P}_s$ from the cladding region to the core region.

Fig. 7 shows the ratios of $P_1 / \bar{P}_s$, $P_2 / \bar{P}_s$ and $P_3 / \bar{P}_s$ for the HE_{11} EH_{11} and HE_{12} modes where P_1, P_2, and P_3 refer to surface wave powers in core, cladding and outer air regions. At higher frequencies, most of the power is concentrated in the core as predicted.

As mentioned before, when we increase the ratio of b : a, there will be more and more modes excited by the scattering center. Mode identification will require more computational time and better programming techniques. This is especially so as γ approaches $\sqrt{\bar{\epsilon}_2}$ (e.g., the $\gamma = 1.50$ line in Fig. 2) where all the cladding modes will asymptotically coverage at higher normalized frequency and where we are close to the transition from the "leaky" modes to the "propagating" modes.

Once $\bar{P}'_s$ for all the scattered modes are established, we have to normalize them to the incident power and scattering volume and express them in terms of dB for comparison with existing data (such as those by Clarricoats and Chan).

As E. Rawson suggested that during pulling of a cladding fibre, some of the impurities will be elongated to become "dielectric needles". This will be studied in the near future, too.

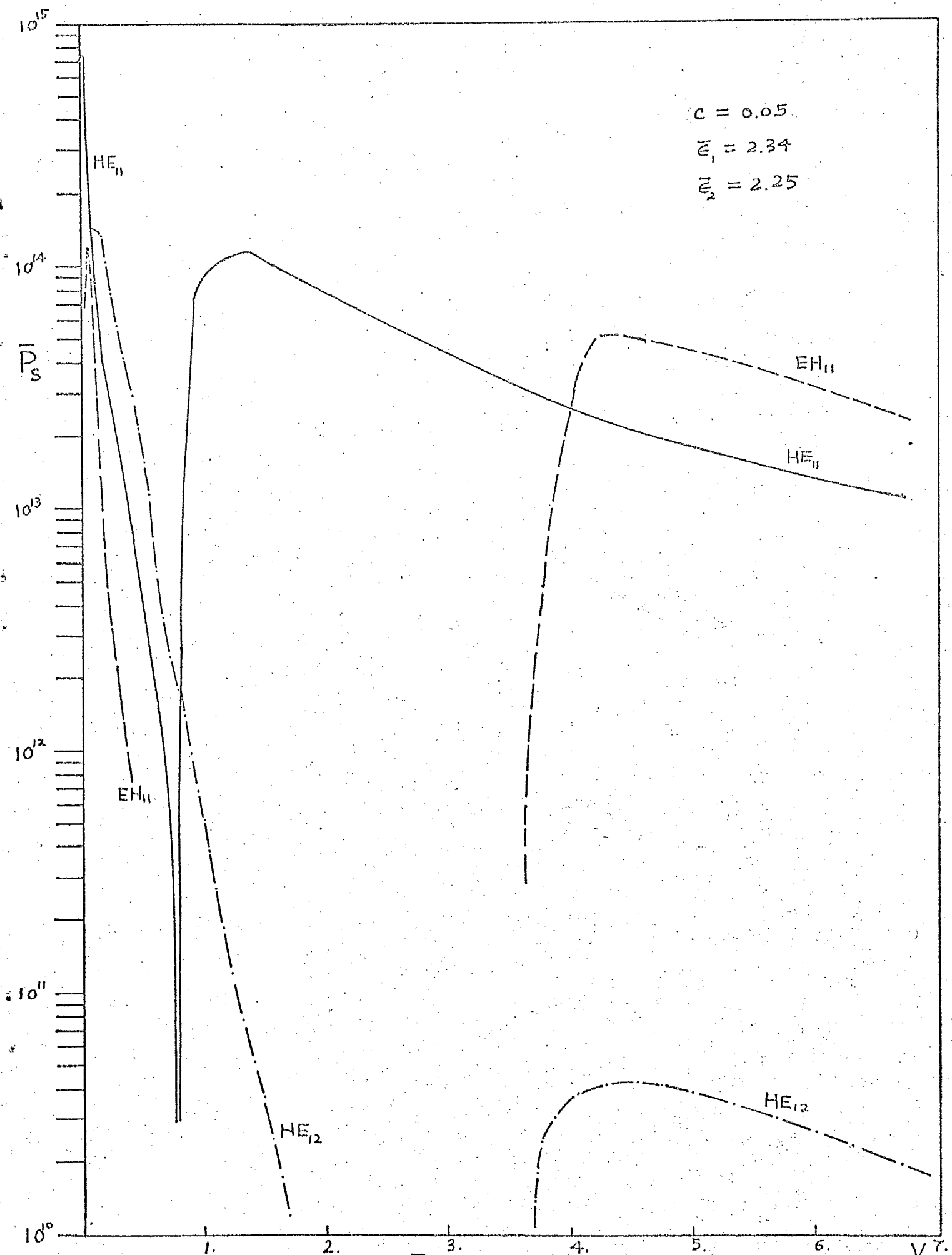

Fig. 6 $\bar{P}_s$ vs. V for the HE_{11}, EH_{11} and HE_{12} modes.

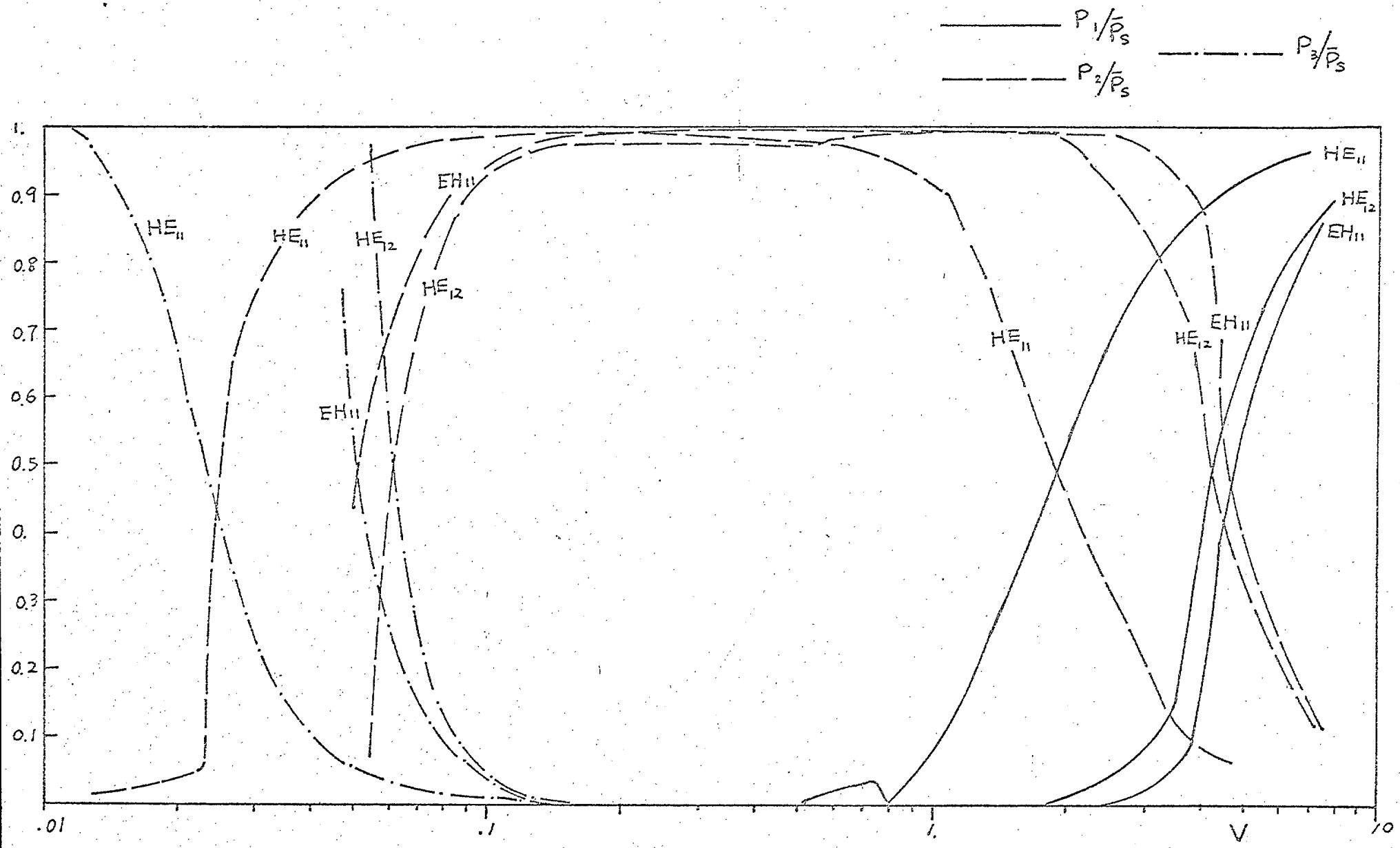

Fig. 7 Mode Conversion Power Ratios for the HE_{11}, EH_{11} and HE_{12} modes vs. V

APPENDIX

Minimum Bend Radius Determined by Critical Angle Criterion

We now derive an approximate expression for the minimum bend radius by using the critical angle criterion. It is assumed that the bend has a negligible effect on the dispersion curves of the guided modes, so that we can use the unperturbed values (γ, V) of the mode spectrum. The geometry is illustrated in Figure 8. Focusing attention on a single core mode ($\theta > \theta_c$), it is seen that in entering the bend these guided core rays leak out into the cladding and hence cause mode conversion. Applying the law of sines on triangle with vertices (1-2-3) gives

$$\frac{R_o}{\sin \theta_b} = \frac{R_o + d_1}{\sin (\pi - \theta)} \quad , \quad d_1 = 2a \tag{A.1}$$

$$\therefore \quad R_o = \frac{d_1 \sin \theta_b}{\sin \theta - \sin \theta_b} \tag{A.2}$$

The critical angle criterion is $\theta_b = \theta_{c1}$

$$\therefore \quad R_o = \frac{d_1 \sin \theta_{c1}}{\sin \theta - \sin \theta_{c1}} = \frac{n_2 \, d_1}{\gamma - n_2} \tag{A.3}$$

on using $\sin \theta_{c1} = \dfrac{n_2}{n_1}$, $\sin \theta = \dfrac{\gamma}{n_1}$ (see Figure 8)

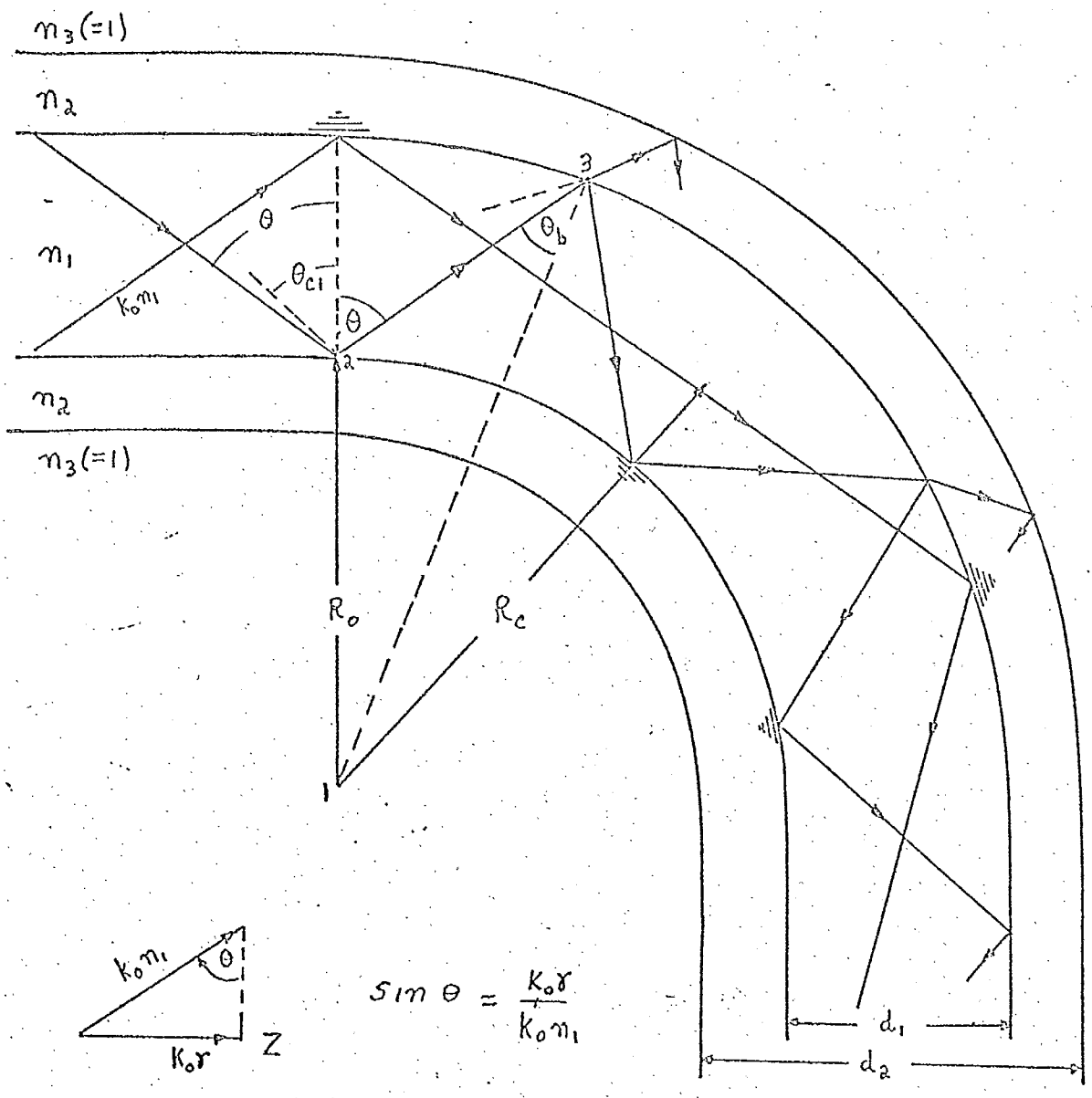

FIGURE 8 Determination of Minimum Bend Radius (R_c) by the Critical Angle Criterion :

$$\sin\theta_{c1} = \frac{n_2}{n_1}$$

$$\sin\theta = \frac{k_0 \gamma}{k_0 n_1} = \frac{\gamma}{n_1}$$

Hence,

$$R_c = R_o + \left(\frac{d_1}{2}\right)$$

$$= \frac{d_1}{2} \frac{(\gamma + n_2)}{(\gamma - n_2)}, \quad \text{for core mode} \qquad (A.4)$$

Equation (2.71) also holds for a cladding mode provided we replace d_1 by d_2, and n_2 by $n_3 = 1$, i.e.,

$$R_c^{(1)} = \frac{d_1}{2} \frac{(\gamma + n_2)}{(\gamma - n_2)}, \quad \text{for } \underline{\text{core mode}} \ (\gamma, V) \qquad (A.5)$$

$$R_c^{(2)} = \frac{d_2}{2} \frac{(\gamma + 1)}{(\gamma - 1)}, \quad \text{for } \underline{\text{cladding mode}} \ (\gamma, V) \qquad (A.6)$$

It is noted that at cut-off, i.e., $\gamma \to 1$, equation (A.6) gives $R_c^{(2)} \to \infty$, which means that power will leak out into the outer medium even though the fibre axis is straight (as expected by the definition of cut-off). Equation (A.5) above shows that, for radii smaller than $R_c^{(1)}$, power from a core mode will be coupled to a cladding mode; whereas equation (A.6) shows that, for radii smaller than $R_c^{(2)}$, power from a cladding mode will be coupled into radiation. In both cases, mode conversion will also take place, since the bend mixes the characteristic angles (θ_{nm}) identifying the guided modes. It should also be observed that a fibre of micron dimensions ($d_2 \sim 10^{-6}$ m) can tolerate sharper bends than one of millimeter dimensions ($d_2 \sim 10^{-3}$ m). This makes the optical fibre more attractive than the millimeter dielectric rod or tube.[11]

No attempt is made here to evaluate the power loss from the waveguide bend. The original intention was only to give some physical insight into the nature of the problem. For more detailed treatments the reader is referred to Gloge[12], Marcuse[13] and Marcatili[14].

REFERENCES

1. D. Marcuse, "Mode Conversion Caused by Surface Imperfection of a Dielectric Slab Waveguide", B.S.T.J., Dec. 1969, p. 3187-3215.

2. D. Marcuse, "Mode Conversion Caused by Diameter Change of a Round Dielectric Waveguide," B.S.T.J., Dec. 1969, p. 3217-3232.

3. K.B. Chan, "Electromagnetic Wave Propagation in Optical Waveguides," Ph.D. Thesis, 1972, University of London.

4. G.L. Yip, "Launching Efficiency of the HE_{11} Surface Wave Mode on a Dielectric Rod," IEEE Trans. MTT. Vol. 18, No. 12, Dec. 1970, p. 1033-1041.

5. G.L. Yip and T. Au-yang, "Launching Efficiency of the HE_{11} Surface-Wave Mode on a Dielectric Tube," IEEE Trans. MTT, Vol. 22, No. 1, January 1974, p. 6-13.

6. D. Marcuse, "Radiation Losses of the Dominant Mode (HE_{11}) of Rounded Optical Fibres," IEE Conf. 1970, No. 71, p. 89-94.

7. A.W. Snyder, "Radiation Losses Due to Variations of Radius on Dielectric or Optical Fibers," IEEE Trans. MTT, Vol. 18, No. 9, Sept. 1970.

8. Eric G. Rawson, "Measurement of the Angular Distribution of Light Scattered from a Glass Fiber Optical Waveguide," Applied Optics, Vol. 11, No. 11, Nov. 1972, p. 2477-2481.

9. Eric G. Rawson, "Theory of Scattering by Finite Dielectric Needles Illuminated Parallel to Their Axes," J.O.S.A., Vol. 62, No. 11, Nov. 1972, p. 1284-1286.

10. A.W. Snyder, "Excitation and Scattering of Modes on a Dielectric or Optical Fiber," IEEE Trans. MTT, Vol. MIT-17, No. 12, Dec. 1969.

11. M.M. Z. Kharadly, J.E. Lewis, "Properties of Dielectric Tube Waveguides," Proc. IEE., Vol, 116, No. 2, p. 214, 1969.

12. D. Gloge, "Bending Loss in Multimode Fibers with Graded and Ungraded Core Index," Appl. Optics, Vol. 11, No. 11, Nov. 1972, p. 2506-2513.

13. D. Marcuse, "Bending Losses of the Asymmetric Slab Waveguide," B.S.T.J., Oct. 1971, p. 2552-2563.

14. E.A.J. Marcatilli, "Bends in Optical Dielectric Guides," B.S.T.J., Vol. 48, No. 7, Sept. 1969, p. 2103-32.

MARTUCCI, J.

Propagation characteristics of optical fibres

DATE DUE
DATE DE RETOUR
